

Faculty of Science Department Physics and Astronomy
Head of Department: Prof. Dr. D. Ryckbosch

A study of early afterdepolarizations in an anatomically correct model of the human ventricles in 3D

Enid Van Nieuwenhuyse

Promotor: Prof. Dr. A. V. Panfilov
Supervisor: Dr. N. Vandersickel

Thesis submitted in partial fulfillment of the requirements for the degree of
Master in Physics and Astronomy

Academic year 2015–2016

Acknowledgement

This thesis would not have been possible without the time, support and dedication of certain people. This is why I would like to express my sincerest gratitude to all of them.

First of all, I am forever indebted to my academic supervisor, Dr. Nele Vandersickel for her enthusiasm and unrelenting support throughout this process. I could not think of a more suitable guidance into the field of research. My progress and growth into a more critical and improved student are her credits. Thank you, Nele. You are the best.

I thank my academic promotor Professor Dr. Alexander Panfilov who gave me the opportunity to conduct this research in his research department. His lessons have been a great introduction to this research, to which I gladly participate.

I would like to thank my family for their unconditioned support and encouragement in the sometimes difficult times. They gave me the opportunity to study and the courage to complete this master. I especially thank my parents for the place they created which we, my siblings and I, can call home. I thank them for their kindness, warmth and patience, but most of all, for the freedom of choice they granted. They were the best role model a child could imagine.

Thank you all,

Van Nieuwenhuyse Enid, june 2016

Admission for usage.

,,The author grants permission to make this master's thesis available for consultation and to copy parts of this master's thesis for personal use. Any other use falls within the limitations of the copyright law, in particular with regard to the obligation to explicitly indicate the source when citing results from this master's thesis."

Van Nieuwenhuyse Enid, june 2016

Samenvatting

In de geïndustrialiseerde wereld behoren hartritmestoornissen en hartaanvallen bij de meest voorkomende doodsoorzaken. Ondanks intensief klinische onderzoek blijven de onderliggende oorzaken vaak ongekend. Het theoretisch onderzoek naar hartritmestoornissen heeft zich in de loop der jaren gevestigd als onderzoekswaarde. Een van de meest belangrijke toepassingen die voortgebracht werd uit dit theoretisch onderzoek, is het simuleren van het menselijke hart. Door gebruik te maken van een mathematisch model, overkomt men veel hindernissen die zich uiten in experimenteel onderzoek. Ten eerste is het niet vanzelfsprekend experimenteel onderzoek te doen op een levend menselijk hart. Alsook kunnen onderzoeken uitgevoerd op dierlijke harten (van honden of cavia's) resultaten opleveren die niet in overeenstemming zijn met biologische of fysiologische eigenschappen van het menselijke hart. Daarnaast zijn klinische waarnemeningen voornamelijk beperkt tot de signatuur aan de oppervlakte van het hart of tijdsafhankelijke metingen zoals een echocardiogram. Wat gebeurt in het centrum van de ventrikels en atria's blijft grotendeels verborgen voor onderzoek.

In de paper ,,A model for human ventricular tissue" [6, 7], wordt het onderzoek onder leiding van Tusscher en Panfilov naar een mathematisch correct model voor ventrikelweefsel beschreven. Het is een hartmodel gebasseerd op experimentele data (onder andere fysiologische waarden van de ventrikelcellen). Het is geschikt voor het simuleren van grote delen hartweefsel. Dit model werd uitvoerig gebruikt in een onderzoek uitgevoerd door Nele Vandersickel. In de paper ,,A study of Early Afterdepolarizations in a Model for Human Ventricular Tissue" [8], toont zij aan dat EADs, een signatuur kenmerkend voor een enkele hartcel, uiting geven tot de vorming van patronen in een ventrikel-weefsellaag. Deze patronen komen tot

stand in verschillende fysiologische domeinen, zonder de aanwezigheid van heterogeniteiten in het computationele-weefsel. Deze patronen werden opgewekt door de fysiologische parameters van het hart stapsgewijs aan te passen. De belangrijkste ionstromen in de hartcellen werden gevarieerd. De vertraagde kalium-ionstroom werd verlaagd en de L-type calcium stroom werd opgehoogd. Dit gaf aanleiding tot 3 verschillende regionen, die zich uiten met een ander patroon. Ze werden geclassificeerd als ,,spiral fibrillation type a SFa, ,,spiral fibrillation type b SFb", and ,,oscillatory excitation regime Osc". Er werd aangetoond dat hartritmestoornissen hun oorzaak kennen als gevolg van deze patroonvorming en dat hartritmestoornissen kunnen onstaan als gevolg van EADs.

Het doel van deze thesis is aan tonen dat gelijkaardige patronen kunnen ontstaan in een driedimensionale voorstelling van het menselijke hart. Met behulp van dezelfde protocols wordt gezocht naar de drie fysiologische regio's. Er wordt alsook aangetoond dat EADs hier ook aan de basis liggen van de verstoorde doorgang van de golf die het hart dient te exciteren voor de initiatie van een hartpuls. Elk regio wordt gekenmerkt door verschillende eigenschappen op cellulair en op groot-schalig weefsel niveau, wat dan ook wordt aangetoond.

Dankzij de collaboratie met de groep van professor Seeman uit Freiburg kunnen we echocardiograms, ECGs, maken van onze patronen. We zullen deze bestuderen en vergelijken met de ECGs van de hartritmestoornis Torsade de Pointes, TdP.

Abstract

Cardiac arrhythmias and sudden cardiac death are among the most common causes of death in the industrialized world. Despite decades of research, their causes are still poorly understood. Theoretical studies into the mechanisms of cardiac arrhythmias form a well-established area of research. One of the most important applications of these theoretical studies is the simulation of the human heart, which is important for a number of reasons. First, the possibilities for doing experimental and clinical studies involving human hearts are very limited. Second, animal hearts used for experimental studies may differ significantly from human hearts. Finally, cardiac arrhythmias, especially those occuring in the ventricles are three-dimensional phenomena whereas experimental observations are still largely constrained to surface recordings or timedependent recordings, like ECG. Computer simulations of arrhythmias in the human heart can well overcome some of these problems.

Studies by Tusscher and Panfilov, described in ,,A model for human ventricular tissue" [6, 7] introduce a widely used model for human ventricular cells based on experimental data and is made efficient for large-scale spatial simulations. In ,,A Study of Early Afterdepolarizations in a Model for Human Ventricular Tissue" [8] numerical studies on this model found that EADs, who normally occur at the level of a single-cell, result in the creation of patterns in certain physiological domains without heterogeneities in the tissue. By reducing the delayed rectifier potassium currents and increasing the L-type calcium current 3 diffrent regions of pattern-formations could be found. They have been classified as spiral fibrillation type b SFb, spiral fibrillation type a SFa, and an oscillatory excitation regime Osc. They showed that arrythmias could be induced in the heart without heterogeneities and that those arrythmias

occur during normal wave propagation disturbed by EADs.

Since cardiac arrythmias are suggested to arise due to this abnormal propagation at the heart-tissue level or are due to malfunctions on the whole-heart level, theoretical research of those malfunctions is a complex problem. As EADs are single-cell behaviour they need to be implemented in the multi-scale mathematical model. Aim of this master's disertation is to follow the same protocols used in the paper [8] and apply them on that mathematical anatomically correct computer-model of the human ventricles in 3D. We will investigate likewise regions of pattern formation by changing prominent ionic currents. We will prove that due to EADs these formations occur and that different regions are characterized with different features.

With the software obtained in collaboration with the group of Professor Gunnar Seemann (Freiburg, Germany), we will be able to create ECGs of the excitation patterns we find. We will study the ECGs and compare them to the ECGs of Torsade de Pointes, hereafter TdP.

Abbrevations

EAD Early Afterdepolarization

SFb Spiral fibrillation type b

SFa Spiral fibrillation type a

Osc Oscillatory type

MS Meandering Spiral

SS Stable Spiral

TdP Torsade des Pointes

ECG Echocardiogram

AP Action Potential

APD Action Potential Duration

HH Hodgkin Huxley

SR Sarcoplasmatic Reticulum

RyR Ryanodine receptors

g conductance

CV Conduction Velocity

RR Repolarization Reserve

AV-node Atrio-ventricular-node

SA-node Sino-atrial node

$V_{membrane}$ Membrane Potential

K Potassium

Na Sodium

P Permeability

I_{KR} Rapid Rectifier Potassium Current

I_{Ca_L} L-Type Calcium Current

VT Ventricular Tachycardia

VF Ventricular Fibrillation

AT Atrial Tachycardia

AF Atrial Fibrillation

Contents

Acknowledgement **ii**

Admission for usage. **iv**

Samenvatting **vi**

Abstract **viii**

Abbrevations **xii**

Index **xiii**

1 The heart as a biophysical system **1**

1. Introduction 1
   - The resting membrane voltage and the Nernst potential. 3
   - Excitability and the action potential AP. 4
2. The Hodgkin-Huxley model for excitable cells. 6
   - The equivalent electrical circuit. 6
   - The HH -model for main ionic currents potassium and sodium 7
   - Qualitative explanation of AP with the HH-model 10
3. The TNNP-TP06 Model for human ventricular tissue. 12
   - Main currents for the AP of the heartcells 12
4. Mathematical Implementation of the equations in the model. 15
5. Early Afterdepolarizations 16
6. Excitation wave pattern formation 17
   - Refractoriness 17
   - Wave-front annihilation 18
   - Competing sources 18
   - Spiral formation 19
7. The electrocardiogram ECG 20
   - Signature of the healty heart on ECG 20
   - Signature of cardiac arrhythmias on ECG 21

2 EAD-induced patterns in 2D **24**
1. SFb, SFa and Osc: 3 wave patterns due to EADs 24
The SFb-type pattern 25
The SFa-type pattern 25
The Osc-type pattern 26
2. Calcium and sodium mediated waves 26
3. Phase waves vs real waves 26
4. ECG and Fouriertransforms 27

3 EAD-induced patterns in 3D **29**
1. Methods 29
S1 pacing 30
S1S2 31
ECG creation 32
2. Results of the S1S2 and S1 pacing protocol 34
3. The SFb, SFa and Osc-type patterns 34
A. Pattern description of SFb, SFa and Osc 34
B. AP profiles 36
C. Mechanisms of pattern formation 38
D. Sodium and L-type calcium mediated waves 41
E. Statistical approach of the AP 42
F. Phase waves versus real waves 44
G. Fourier transforms 44
H. ECGs 46
4. The meandering spiral 49
A. Mechanisms of pattern formation 49
B. ECGs of the meandering spiral 50

4 Discussion **53**
The SFb-, SFa- and Osc-type excitation patterns in 3D. 54
SFb 54
SFa 54
Osc 54
The meandering spiral and Torsade de Pointes 55

Bibliography **59**

List of Figures **63**

List of Tables **68**

Chapter 1

The heart as a biophysical system

1. Introduction

The heart is the center of the circulatory system, which provides blood to the body tissues, delivering nutrients and oxygen, needed for the health and functions of each individual cell. It's main function is mechanical and it works like a pump. The human heart consists of four chambers. The upper ones, the atria, and the lower ones, the ventricles. The atria collect the blood and after their contraction they push the blood into the ventricles. Afterwards, the ventricles, build with large cardiac walls up to 2.0 cm, contract and force the blood out the heart. Those contractions are initiated by the sinoatrial node, SA-node, located in the right atria.

Cardiac muscle cells are excitable due to their resting membrane potential. As they have a non-zero electrical potential, they can react on external applied electrical stimuli. The cells located at the SA-node differ from the normal cardiac cells, as they are able to depolarize spontaneously. They are called the pacemakercells of the heart as they determine the heart-rate. They repeatedly undergo a cycle, by which they change their membrane potential. The voltage-signature of the pacemakercells is shown in Figure 1.1. Due to the electrical connection between the pacemaker and atria cells, by gap-junctions and (ion)channels connecting cellwalls, the depolarizing excitation wave initiated by the spontaneous depolarization of the pacemakercells will propagate through the atria and excite the cardiac cells; the cardiac cells are pushed over a certain threshold by which they undergo their own typical action potential AP (Figure 1.1). After the wave has spreaded, the atria contract.

In order to pump efficiently the atria need to contract first to collect the blood from the body and push it into the ventricles. Therefore the atria and ventricles are not electrically connected. The only point where the electrical impulse can be passed from the atria to the ventricles is the atrio-ventrical(AV)-node. This electrical disconnection provides the atria the

time to contract. This delay can take up to 0.1 seconds but results in a stronger bloodflow in the body. With internodal pathways the AV-node is connected with the AV-bundle passing on the electrical signal. The AV-bundle branches into a left and right bundle. They consist out of Purkinje fibers. The fibers are large and the heart needs them for their fast transportation of the AP (up to 4.0 m per second). Due to the fast transportation, a rapid and homogeneous excitation of all cardiac cells in the ventricular tissue is possible. This makes contraction in the ventricles coherent.

Figure 1.2 shows the prominent structures, described above, within the heart, whom are responsible for the spreading of the excitation wave. Figure 1.3 shows qualitatively how you can imagine the wave spreading through the heart.



Figure 1.1: Comparison of the AP of the pacemaker cells and normal cardiac cells. The pacemaker-cells depolarize spontaneously. The normal cardiac cells need an external applied stimulus or electrical pulse in order to push them over excitation threshold.

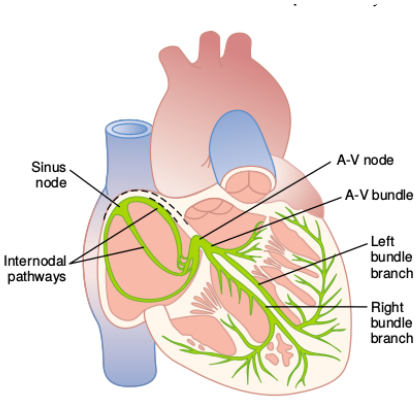


Figure 1.2: Anatomical pathway of spreading of the electrical excitation wave from AV-node to ventrical cardiac tissue, from Medical Physiology, Guyton and Hall.

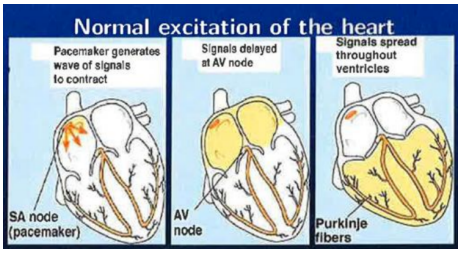


Figure 1.3: Spreading of the electrical excitation wave from AV-node to ventrical cardiac tissue, from Waves and patterns in biophysics, A. Panfilov.

The resting membrane voltage and the Nernst potential.

The intracellular and extracellular ion-concentrations of the human cell differ significantly, as shown in Tabel 1.1. The cell membrane possesses different ionic channels through which ions can migrate. Hence, the ions are aware of the lower/higher concentration on the other side of the membrane. In case the molecules would not posses electrical charge, they would diffuse through the other side until equilibrium due to diffusion has settled. Since we consider charged ions, the conditions for equilibrium differ as moving electrical charges change the electrical potential at both sides of the membrane and thus create an electrical field.

Element	Ion	Extracellular	Intracellular
sodium	Na^+	142	10
potassium	K^+	4.0	140
chloride	Cl^-	103	4
calcium	Ca^{2+}	2.4	10^{-4}

Table 1.1: Intra- and extracellular concentrations of main ions in mM, from Medical Physiology, Guyton and Hall.

Let's consider the case where only potassium can move through the membrane. There is a large concentration inside the cell which will diffuse due to the concentration gradient. For each potassiumion which migrates through the membrane, the intracellular fluid will become slightly negatively charged while the extracellular fluid becomes slightly posititvely charged. This induces an electrical field, pushing other positively charged K^+-ions back inwards. At some point, the cell will reach an equilibrium, when a certain electrical field and a certain gradient-flow will keep each other in balance. This results in a stationary potential, defined by the difference between the electrical potential inside and the electrical potential outside $\phi_i - \phi_o$. This is called the membrane potential $V_{membrane}$. If we assume the cell contains enough ions

ensuring electro-neutrality, this membrane potential will be equal to the Nernst potential of potassium. Theoretically, the Nernst potential for a certain ion is given by Formula 1.1:

$$V_{Nernst} = -\frac{RT}{zF} ln \frac{c_i}{c_o} \tag{1.1}$$

where c_i/c_o denotes the intracellular/extracellular concentration of the ion of interest, here thus potassium. With R, the universal gas constant, equal to 8.314 J/K mol, F the Faraday constant, equal to $9.648*10^4$ C/mol, $V_{Nernst,K}$, at a room temperature of 25° Celsius, lies around -100 mV.

As the membrane is permeable for different ions, each ion will diffuse through the membrane, creating a diffusion gradient and adjoining electrical field. Depending on the difference between intra- and extracellular concentrations, the ions will flow either outwards or inwards. Both sodium and chloride ions, for example, flow inwards. As each ion will try to reach its own Nernst potential, the cell will not reach an equilibrium, as the Nernst potential of one ion will induce diffusion of other ions.

Though it is possible to search for a membrane potential by assuming that the inwards and outwards current neutralize each other. In that case, the total current through the membrane is set to zero. This membrane potential can be found with the use of the GHK-equation, which takes into account the presence of multiple ions and takes the different permeabilities of each different ion-channel into consideration. The GHK-equation reads (Formula 1.2):

$$V_{membrane} = -\frac{RT}{F} ln \frac{\sum^{z=+1} P_i c_i + \sum^{z=-1} P_j c_o}{\sum^{z=+1} P_i c_o + \sum^{z=-1} P_j c_i} \tag{1.2}$$

where the summation runs over each ion, with either a positive or negative unit-charge (only $|z|$=1 has been taken into account in the calculations). If we consider the main ion-compontents of the cell, potassium and sodium, as their influence determines the global form of the AP, we get:

$V_{membrane} = -25mV(ln\frac{P_{Na}c_{Na_i}+P_K c_{K_i}}{P_{Na}c_{Na_o}+P_K c_{K_o}})$

which results in $V_{membrane}$ = -88.53 mV.

Excitability and the action potential AP.

The membrane potential $V_{membrane}$ = -88.53 mV is indeed a good approximation of the real resting potential of the cardiac membrane. As can be seen, this value is very close to the Nernst potential of potassium, which is due to the fact that the permeability of sodium P_{Na} at a voltage of -90 mV is much smaller than the permeability of potassium P_K. Due to the lower permeability, the sodium ions have it less easy to diffuse through the membrane and mostly potassium will determine the behaviour of the membrane potential. If however the

cardiac cell slightly depolarizes due to external influences, P_{Na} increases fastly, pushing the membrane-potential to the Nernst potential of sodium, which with the use of Formula 1.1 can be found to be around +60 mV. This jump is fast and takes around a millisecond. However, after this quick raise of the potential, the permeability of the sodium channels reduces again and potassium channels will restore the potential. Figure 1.4 schematically represents the influence of sodium and potassium in the creation of AP. The total time of one AP is around 300 milliseconds for cardiac cells.
When the pacemakercells in the SA-node depolarize, their AP is pushed to the Nernst potential of sodium. This local potential change spreads as the depolarization of the potential induces the sodium-gates in adjecant cells to open. After those cells start to depolarize, they raise the potential in their neighbourhood. Like this, an excitation wave spreads through the atria, making it possible for the atria to contract and sending the electrical pulse through the AV-node to the ventricles.

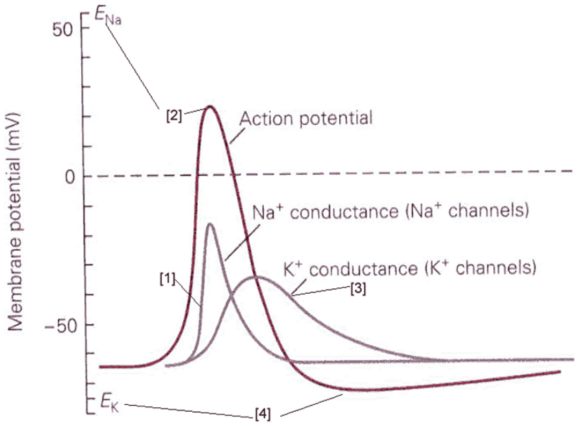


Figure 1.4: Illustration of the influence of potassium and sodium on the global formation of the AP.

It's clear that this single-cell behaviour can be very complex. The form of the AP is not only determined by the ionic concentrations in the intra- and extracellular fluid but also by the time and voltage dependency of the permeability of the channels which control the ionflows through the membrane. In 1952, Hudgkin and Huxley introduced a mathematical approximation to capture the physics of the channels. Combining the differential equations of these channels into a model, they were able to describe the dynamical plane of APs.

2. The Hodgkin-Huxley model for excitable cells.

The equivalent electrical circuit.

The cell membrane separates the intra- and extracellular fluids from each other. This membrane is built out of a lipid bi-layer, where the ions can flow through the membrane thanks to the channels, built out of certain proteins. The largest part of the lipid bi-layer acts as an insulator for the electrical charges. As the layer stores ions at both sides, it resembles the behaviour of an electrical capacitor. Based on earlier results they had found, Hodgkin and Huxley published a paper [5] were they collected those results and described a mathematical approximation of the electrical nature of the excitable cells.

They started with dividing the total membrane current I, into a capacity current with a membrane capacity per unit area C_M, and the ionic current density of the ions moving through the channels I_i. They placed both elements in parallel, based on their experimental results, which resulted in Formula 1.3 :

$$C_M \frac{dV}{dt} + I_i = I \tag{1.3}$$

where C_M is assumed to be constant, V is the displacement of the membrane potential from its resting value, t is time, I is the total membrane current density and I_i is the ionic current density. As potassium and sodium ions determine the global behaviour of the AP, they introduced time- and voltage-dependent potassium and sodium currents, I_K and I_{Na}, and one collective leakage current I_l, due to chloride and other ions, assumed to be constant. Figure 1.5 shows a clear overview of the electrical circuit of the membrane.

They tried to represent their results of the patch-clamp experiments on the nerve of a giant squid with the help of 3 equations describing the different behaviour of each individual current (Formulas a, b, c of 1.4):

$$\begin{aligned} I_{Na} &= g_{Na}(V - V_{Na}) \qquad (a) \\ I_K &= g_K(V - V_K) \qquad (b) \\ I_l &= \overline{g_l}(V - V_l) \qquad (c) \end{aligned} \tag{1.4}$$

with V, the present displacement at time t from the resting potential of the membrane and V_{Na}, V_K and V_l the displacement from the Nernst potentials of each individual ion and the value of the resting potential of the membrane:

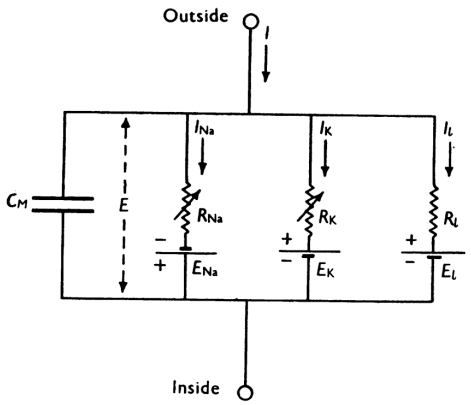


Figure 1.5: Equivalent electrical circuit representing the dynamics of the membrane. Resistances R_{Na} and R_K are time and membrane potential dependent, R_L is constant, from the original paper of A. L. Hodgkin and A. F. Huxley

$$V = V_t - V_{membrane_{rest}}$$
$$V_{Na} = V_{Nernst_{Na}} - V_{membrane_{rest}}$$
$$V_K = V_{Nernst_K} - V_{membrane_{rest}}$$
$$V_l = V_{Nernst_l} - V_{membrane_{rest}}$$

This made it more easy to interpret the patch-clamp results: electrodes where applied outside and inside the nerves of the giant squid. After applying a voltage difference, the membrane reacted with a certain time-course τ. Each different channel could be studied by blocking other channels with drugs and applying different voltage-jumps. An example of such a patch-clamp experiment is presented in Figure 1.6. In these experiments, they have gradually raised the voltage jump: $V - V_{ion}$. Each time the jump has been applied, the conductance g of the channel changed and they modelled the ion-current by Formulas 1.4.

The HH -model for main ionic currents potassium and sodium

potassium

Based on their patch-clamp results, represented in Figure 1.6, they noticed that the potassium conductance g_K increases with a slight delay when the nerve is depolarized, an inflection point, but when it returns to its resting voltage there is not an inflection point noticeable. Mathematically it is possible to fit a first-order equation to the ,,closure" of the channel, but the inflection point needs a third- or fourth-order equation in order to describe it correctly. Hodgkin and Hyxley achieved a good fit by supposing that g_K is proportional to a fourth power of a variable which obeys a simple first-order equation. This can give an inflection

point at the beginning, $(1-e^{-t})^4$, but can fall of exponentially e^{-4t}. Thus they separated the conductance g_K into a factor $\overline{g_K}$, a constant with dimensions of conductance $/cm^2$ and also the largest value of the conductance and n, a dimensionless variable varying between 0 and 1. n is the variable obying the first-order equation. In order to describe the voltage-dependency of n they introduced α_n and β_n, rate constants which vary with voltage but not with time as a first order time-dependency for n was assumed. The dimensions of the rate constants are t^{-1}. The formulas read:

$$\begin{aligned} g_K &= \overline{g_K} n^4 \qquad (a) \\ \frac{dn}{dt} &= \alpha_n(1-n) - \beta_n n \qquad (b) \end{aligned} \tag{1.5}$$

which can be solved as

$$\begin{aligned} n &= n_\infty - (n_\infty - n_0)e^{-t/\tau} \qquad (a) \\ n_\infty &= \frac{\alpha}{\alpha+\beta} \qquad (b) \\ \tau &= \frac{1}{\alpha+\beta} \qquad (c) \end{aligned} \tag{1.6}$$

Comparing the experimental results with this mathematical description (shown in Figure 1.7), we see that the experimental results (full lines) do not follow exactly the inflection point of the experimental results (with dots). Hodgkin and Huxley could take a higher order, but the gain was not compensated by the higher complexity. They gave the theoretical results a physical basis by assuming the membrane needs four similar subunits to occupy the channel before the potassium-ions could cross the membrane. If we assume n to be the amount of subunits inside the membrane and (1-n) the amount of subunits outside, the change of the concentration of subunits inside is given by Formula 1.5 (b). With a rate of β_n subunits leave, and with a rate of α_n, they flow in. In [13], it turned out that indeed, there are 4 proteins needed creating the channel on the membrane before transport is possible.

Most importantly, with the help of their mathematical description, the complex time- and voltage dependent permeability of the potassium gate could be captured in an equation by the help of their experimental knowledge of the dependency of α and β. As can be seen in Formula 1.6 (a) and (b), the saturation time τ and final saturation value n_∞ depend on α and β. Figure 1.7 illustrates the time- and voltage- dependency of the potassium gate. The saturation time τ and the final potassium conductance g_∞ differs obviously at different applied external stimuli. At high applied voltages, the conductance saturates much faster. As applying an external voltage results in an increase of the potassium current, n is called an activating gate.

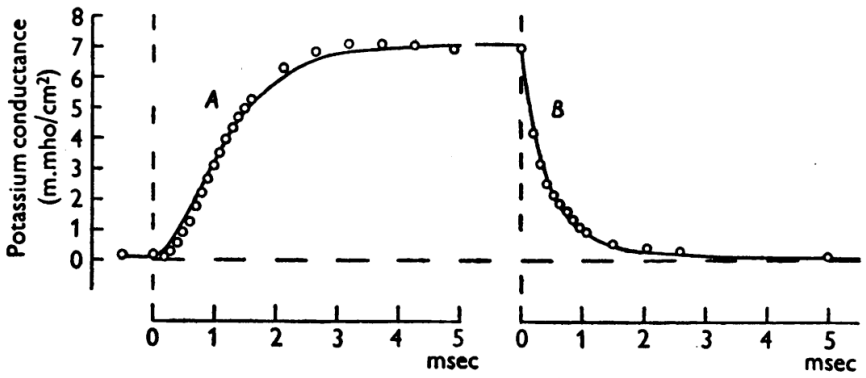


Figure 1.6: A, raising g_K associated with depolarization. B, reducing g_K associated with repolarization of the membrane, from the original paper of A. L. Hodgkin and A. F. Huxley.

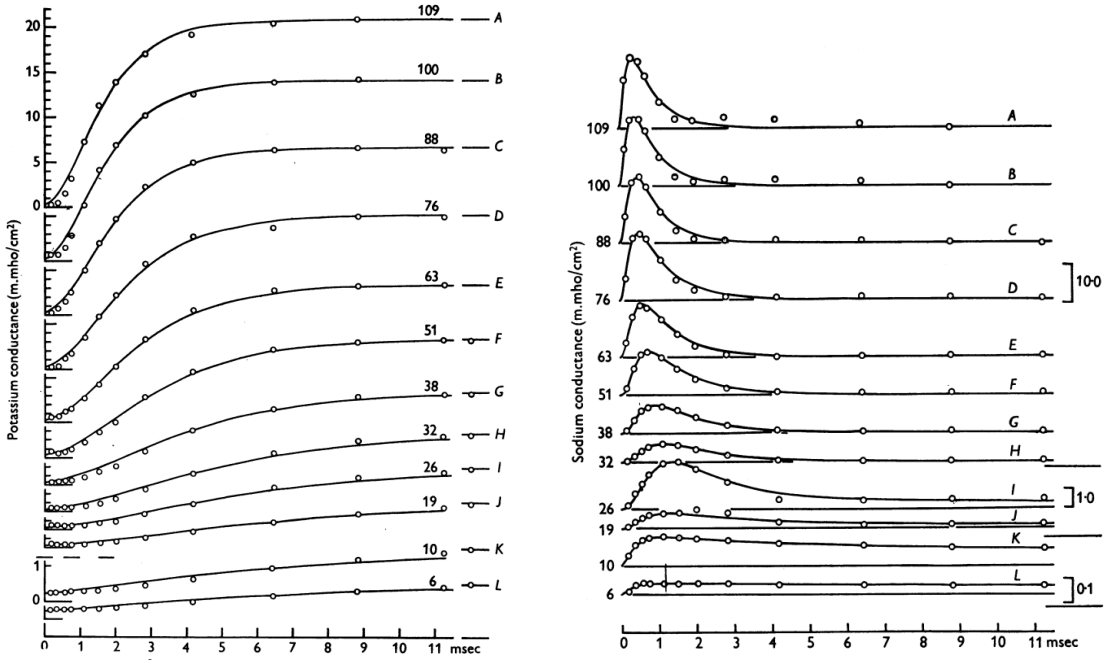


Figure 1.7: Left: Determination of the dependency of the potassium channels on both voltage and time; the time scale applies to all records, the ordinate scale is the same in the upper ten curves (A to J) and is increased fourfold in the lower two (K and L), the number is the depolarization in mV. Right: Determination of the dependency of the sodium channels on both voltage and time, the time scale applies to all records, the ordinate scale is the number of the depolarization in mV. From the original paper of A. L. Hodgkin and A. F. Huxley.

Sodium

To mathematically describe the sodium channel, they introduced 2 variables. One responsible for the opening of the sodium channel, resulting in a raise of the conductance and one responsible for the closure of the sodium channel, and thus the decreasing conductance, as can be seen in Figure 1.7. m, is called the activating gate, h is called the inactivating gate. The conductance clearly shows a dependency on both voltage and time. Both variables m and h are dimensionless, obeying a first-order equation:

$$\begin{aligned} g_{Na} &= \overline{g_{Na}} m^3 h && (a) \\ \frac{dm}{dt} &= \alpha_m(1-m) - \beta_m m && (b) \\ \frac{dh}{dt} &= \alpha_h(1-h) - \beta_h h && (c) \end{aligned} \tag{1.7}$$

whereas with the case of potassium, the α's and β's are voltage dependent, but not time-dependent. Depending on the applied voltage, the gates will have a characteristic saturation time τ and a saturation value m_∞ and h_∞ determining the typical course of the gate in the records of Figure 1.7.

Analogously to the potassium channel, it is possible that several subunits are needed in order for the gate to open. For the opening of the gates, you can assume you need 3 subunits, where (1-m) is the concentration outside and m is the concentration inside of those subunits. For the closure, you can assume to need 1 subunit at the membrane with a concentration of (1-h) outside the cell and h inside the cell. However this does not show in physical experiments. The model to describe the sodium-channel is thus merely mathematical.

Qualitative explanation of AP with the HH-model

Both channels were put together with the leakage current I_l. Hodgkin and Huxley thus succeeded to mathematically describe the dynamics of the excitability of the cell. The equations of the model are given by Formula 1.8

$$C_M \frac{dV}{dt} = -\overline{g_K} n^4 (V - V_K) - \overline{g_{Na}} m^3 h (V - V_{Na}) - \overline{g_L}(V - V_L) \tag{1.8}$$

and Formulas 1.5, 1.6 and 1.7. Each individual channel is characterized with its own activating and for sodium also inactivating constants. From the analysis of the data collected in the two graphs in Figure 1.7, it follows that the time constant of the activating sodium channel is order 10 lower then the ones of potassium or the closing gate of sodium. The activating gate of sodium thus opens very vast, pushing the AP to the Nernst potential of sodium. Qualitative, we can describe the AP as follows:

Step 1 The membrane is in rest at the resting potential, mostly determined by the Nernst potential of potassium. For the gates, this is represented in the first graph of Figure 1.8. Both activating gates, m and n are closed and the inactivating gate h is open.

Step 2 From the moment the membrane senses a slight depolarization in its environment, the activating gate m, quickly opens. As the gates n and h have higher time-constants, they open slower. The Na-channel becomes permeable and sodium-ions flow inside. The cell reaches the Nernst potential of sodium (second graph of Figure 1.8).

Step 3 After a while, the n-gate opens and h-gate closes. Resulting in a higher current of potassium-ions flowing outside, and the h-gate hinders the sodium-flow. The exciting power of the Na-ions disappears and the membrane potential repolarizes to its resting value, where the initial conditions are restored (the last step in Figure 1.8).

AP The behaviour of the conductances of potassium and sodium is represented in Figure 1.9. We see the formation of the AP. This based on mathematical approximations. A model for theoretical determination of the AP of a membrane has been founded.

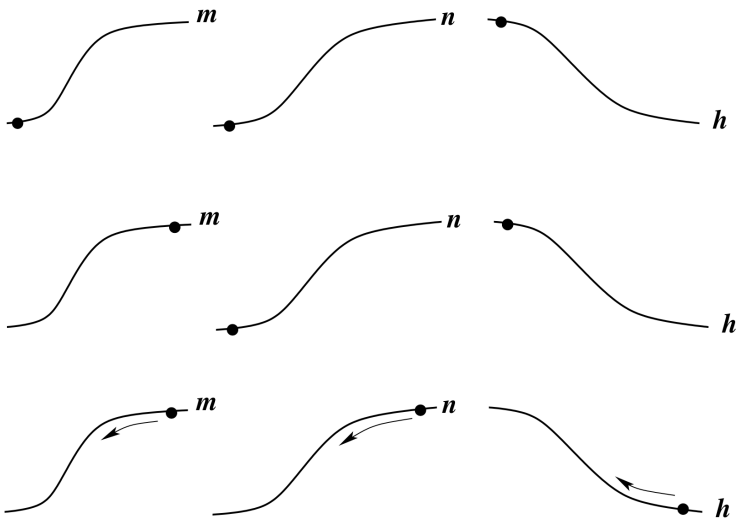


Figure 1.8: Illustration of step 1, 2 and 3 in the formation of the AP, from Waves and patterns in biophysics, A. Panfilov

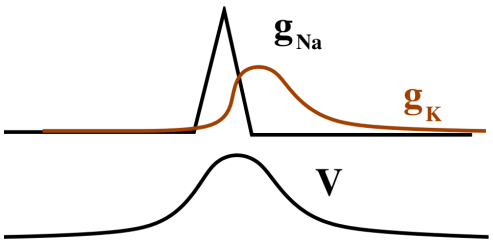


Figure 1.9: Simplified representation of the influence of the sodium and potassium channels, from Waves and patterns in biophysics, A. Panfilov

3. The TNNP-TP06 Model for human ventricular tissue.

In the papers ,,A model for human ventricular tissue" [6] and ,,Alternans and spiral breakup in a human ventricular tissue model" [7], Ten Tussher, K.H.W.J.,D. Noble, P.J. Noble and A.V. Panfilov introduce a model for human ventricular tissue. It is a widely used model for large-scale spatial computations of reentrant sources of cardiac arrythmias. The model reproduces the detailed properties of a single human ventricular cell, such as the main ionic currents; the fast sodium current I_{Na}, the L-type calcium current I_{Ca_L}, the transient outward current I_{to}, the rapid delayed rectifier current I_{KR}, the slow delayed rectifier current I_{KS} and the inward rectifier potassium current I_{K1}. The model also reproduces the AP duration (APD) and important properties of wave propagation in human ventricular tissue, such as the conduction velocity CV: the speed of the wave spreading through the ventricular tissue. Despite this detailed properties of each ionic channel for each cell, they succeeded in creating a model which is computationally efficient enough for large-scale spatial simulations.

Main currents for the AP of the heartcells

In order to reproduce correctly the single cell behaviour of the model, they introduced more currents then the ones we already discussed. In Figure 1.10 we mark the most important currents and the direction in which they flow. As described before, there is the sodium(I_{Na})-current and the potassium(I_K)-current. Also the L-type calcium (I_{CaL}), potassium 1 (I_{K1}) (inwards oriented currents), the transient-outwards (I_{TO}), rapidly activating recitfier potassium current (I_{KR}) and slowly activating rectifier potassium current (I_{KS}) (outward currents) are added to the model. Each of this currents play an important role in the formation of the single cell AP and for the APD, which for a cardiac cell is around 300 ms.

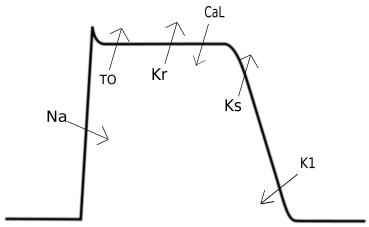


Figure 1.10: Main currents responsible for the typical form of the cardiac AP. The direction of the arrows denotes if the current is either outwards or inwards.

Sodium current I_{Na} As described before, the sodium current is a depolarizing current, pushing the AP to the Nernst potential of Na, at around +50 mV. It has a very fast activating gate and is responsible for the onset of the AP. The sodium current is the largest of all currents. It moves the larges amounts of ions through the membrane. Therefore, changes in its conductance or activation/inactivation properties due to biological mutations or drugs can have profound consequences for the heart and thus the individual.

Transient outward current I_{TO} It is an outwardly directed potassium current with fast activating and inactivating gates and plays thus an important role in the very beginning of the AP, shortly after the upstroke due to sodium. It's repsonsible for the creation of the notch in the AP-curve.

Rapidly and slowly activating rectifier potassium current I_{KR} **and** I_{KS} Outwardly directed currents which, as described before, try to push the AP back to the Nernst potential of potassium, at around -90 mV. The interplay of this current with the L-type calcium current create the typical plateau-phase of the AP. Mainly the rapid current will play an important role. The slowly activating current is slower and will only be activated if the rapid current is blocked. In order to keep the extracellular concentration of potassium and the intracellular concentration of sodium high enough for the cell to be excitable, there is a NaK-pump, pumping the ions against their diffusion gradient.

Potassium K1 current I_{K1} An inward directed potassium current which plays a role at the very end of the AP. It's responsible for the notch in the end and has a strong rectifying feature.

L-type calcium current I_{Ca_L} As calcium is deadly for the cell, the cell tries to keep the intracellular calcium-concentration as low as possible. But, for cardiac contraction, the heartcell needs a large amount of the ion. Due to the CICR(,,calcium-Induced-calcium-Release") reaction chain, whereby a slight concentration change of the intracellular calcium-concentration induces a release of calcium from the storage place in the cell, the sarcoplasmatic reticulum

SR, the intracellular calcium concentration can be raised fastly. Differing from the other cells where the ion-concentrations changes are rather small, the concentration change during AP of calcium is large. Therefore the calcium-dynamics is more difficult to represent mathematically than the other currents. Figure 1.11 illustrates the complexity of the dynamics in the heartcell. In order to keep the intracellular concentration of calcium as low as possible, the cell collects the SR around the T-tubulus. These T-tubules are small slots in the membrane, containing a lot of Ca-channels, through which the ions can migrate from the extracellular to the intracellular environment. From the moment the voltage-sensitive channels open, calcium flows into the cell, raising the intracellular concentration, locally in the neighbourhood of the SR. The calcium triggers the ryanodine receptors (RyR-receptors) on the SR, which signal the SR to release the calcium. It's a positive feedback system. After the cell contracted, the ions are pumped back in the SR and to the extracellular fluid with the aid of the NCX-pump. The natricum-calcium exchanger pump will depending on the phase of the AP either pump sodium inwards and calcium outwards, or, sodium outwards and calcium inwards. An important change of the model of [6] in [7] was this more accurate description of the complex dynamics in the heartcell by introducing a subspace in the model. The CICR current was introduced and the L-type calcium current firstly injects calcium into the subspace instead of the intracellular environment.

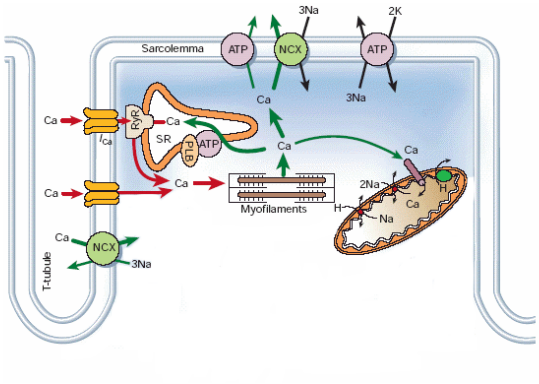


Figure 1.11: Representation of the different aspects responsible for the complex dynamics of calcium in the cardiac cell.

Other currents Also a current for the NCX-pump, the NaK-pump and calcium and potassium plateau currents are added. The NCX-pump pumps the calcium back into the SR or to the extracellular fluid. The NaK-pump works against the gradient of sodium and potassium in order to keep the intra- and extracellular concentrations of both those ions high enough so the cell stays excitable. Finally also a calcium and sodium background current were added to the model.

4. Mathematical Implementation of the equations in the model.

As explained before, the cell can be mathematically represented by an electrical circuit. Thus, in this model, the cell membrane is also modeled as a capacitor connected in parallel with variable resistances and batteries, whom represent the different ionic currents and pumps. The single cell behaviour is described by the differential equation

$$C_m \frac{dV}{dt} = -I_{ion} - I_{stim} \tag{1.9}$$

where, as before, V is the voltage, t is time, I_{ion} the sum of all transmembrane ionic currents which we described above, I_{stim} the externally applied stimulus current and C_m the capacitance per unit of surface area. As the excitation wave travels fastly over a large distance in the heart, the discrete heartcells can be considered as a contineous medium. Therefore, a 2D sheet of cardiac tissue can be modelled as a contineous system with a partial differential equation given by:

$$\frac{\partial V}{\partial t} = -\frac{(I_{ion} + I_{stim})}{C_m} + \frac{1}{\rho_x S_x C_m}\frac{\partial^2 V}{\partial x^2} + \frac{1}{\rho_y S_y C_m}\frac{\partial^2 V}{\partial y^2} \tag{1.10}$$

with ρ_x and ρ_y the cellular resistivities in the x and y direction, S_x and S_y the surface−to−volume ratios in the x and y direction and I_{ion} the sum of all transmembrane ionic currents given by:

$$I_{ion} = I_{Na} + I_{K1} + I_{to} + I_{Kr} + I_{Ks} + I_{Ca_L} + I_{NaCa} + I_{NaK} + I_{pCa} + I_{pK} + I_{bCa} + I_{bNa} \tag{1.11}$$

The value of C_m was set to 2.0 $\mu F/cm^2$ and the surface−to−volume ratio S was set to 0.2 μm^{-1} [34]. In order to reach a maximum planar CV of 70 cm/s a cellular resistivity $\rho = 162$ Ω cm was requierd, which resulted in a diffusion-coefficient D $=\frac{1}{\rho S C_m}$ of 0.00154 cm^2/ms
The implementation of the currents happened in a Hodgkin-Huxley type manner. The 2 currents which we will vary in this thesis are the L-type calcium and the rapid rectifier potassium current and are implemented as :

$$I_{Ca_L} = G_{Ca_L} df f_2 f_{cass} 4 \frac{(V-15)F^2}{RT} \frac{0.25 Ca_{ss} e^{2(V-15)F/RT} - Ca_o}{e^{2(V-15)F/RT} - 1} \tag{1.12}$$

$$I_{KR} = G_{Kr}\sqrt{\frac{K_o}{5.4}} x_{r1} x_{r2} (V - E_K) \tag{1.13}$$

In this first equation d, f, f_2 and f_{Cass} represent the gating variables as described before in the Hodgkin-Huxley model. d is a voltage-dependent activation gate, f_{Cass} is a fast-subspace calcium-inactivation gate, f is a slow, voltage-inactivation gate, and f_2 is a fast, voltage-inactivating gate. Fast and slow gates are distinguished by their time constants. For the

second equation, x_{r1} is the activation gate and x_{r2} is the inactivation gate. E_K denotes the Nernst potential of potassium. G_{Ca_L} and G_{KR} denote the maximal conductance for either the L-type calcium current and the rapid rectifier potassium current with a value of 0.00003980 $mm^3/(ms\mu F)$ respectively 0.1532432 $\eta S/pF$ as default. Another used current in order to obtain certain results is the I_{Na} and is implemented as

$$I_{Na} = G_{Na} m^3 hj(V - E_{Na}) \tag{1.14}$$

where m is the activating and h the fast inactivating gate as described in the Hodgkin-Huxley model of section 2. In this model, also an other gate is added, namely the j-gate. It is a slowly inactivating gate to account for the recovery of the sodium gate whose influence comes to expression when the frequency of the applied pulses becomes high. We refer the reader for a more detailed description of all currents to [6, 7].

5. Early Afterdepolarizations

Early afterdepolarizations (EADs) are depolarizations during the repolarizing phase of the AP. It thus results in an abnormal time course of the AP. EADs emerge at the single-cell level and are a result of mutations or changes of properties of the individual ionic channels [33]. Figure 1.12 illustrates the emergence of an EAD during the AP of the cell.

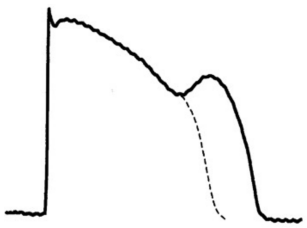


Figure 1.12: Illustration of an EAD.

EADs emerge when the repolarization reserve RR is decreased. The concept of RR was introduced by Roden et al. [14–16]. Multiple studies showed that the reduction of RR increases the likelihood of generating EADs. With the TNNP-TP06 model [6, 7], we will reduce the RR by reducing outward currents like I_{KR}, I_{KS}, .. and raise inward currents like I_{Ca_L} to induce EADs.

6. Excitation wave pattern formation

EAD APs differ substantially from normal APs. It is well established that the emergence of EADs is associated with increased arrhythmogenicity: prone to induce arrhythmias. This higher arrhythmogenicity shows by producing ectopic beats (see section 7) which can initate an abnormal heartcontraction. Also, EADs can augment the electrical heterogeneity in the heart, which also raises the arrhythmogenicity [17, 18].

Therefore, understanding the influence of EADs on the complex pattern formation of the excitation waves in the heart is of great importance. In this thesis, we will study the influence of EADs on the spatial excitation patterns in an anatomical model of the ventricles in 3 dimensions. At first, we thus need to know the basic features of the excitation waves. In this section we shortly describe the mathematical characteristics of these waves and how a spiral can be induced in the heart.

Refractoriness

Consider the excitation wave in the heart. As explained before, the membrane potential of the cell lies at -90 mV. From the moment a single cell repolarizes, the sodium channels become highly permeable and push the membrane voltage to an excited state at +50 mV. As can be seen in Figure 1.18 (left), this upstroke takes very little time in comparison with the 300 ms of the total AP. The upstroke of the AP propagates through the tissue, changing each cell from one state, the resting state determined by the potassium-ions, to another state, the excited state determined by the sodium-ions. A wave like this can be called a trigger-wave. This could be visualized more easy by considering the combustion front of a fire along dry grass-planes. At first, it warms up the grass in front of it, until the grass has reached a certain treshold where it sets on fire. After the combustion front, the grass will be burned down. The front thus changes the grass from a green vivid state to a state of ashes. An important feature of these two trigger waves is a refractory period after the passage of the front. When the fire has passed, the ashes can not sustain a new fire-wave. The grass has lost its excitability when it has changed from the green to the black state. Likewise, after the front has left a region of tissue in the high voltage state, a new depolarizing wave can not travel through it because the cells are still excited and the wave will stop. We illustrate the wavefront and refractoriness of the tissue in Figure 1.13 on the left. You can see a wavefront in red, travelling through the white region in one state, and after the passage of the front, the region is left in a green, excited state, which has lost excitability. In case the medium has the possibility to recover from the excited state back to the resting state, it will be able to sustain a new wave. The time between the passing of the wavefront and the ability to sustain a new one is called the refractoriness of the medium. For cardiac cells this is equal to the time needed for the AP to repolarize to the resting potential state. As seen on Figure 1.18 this is around 300 ms and is

called APD.

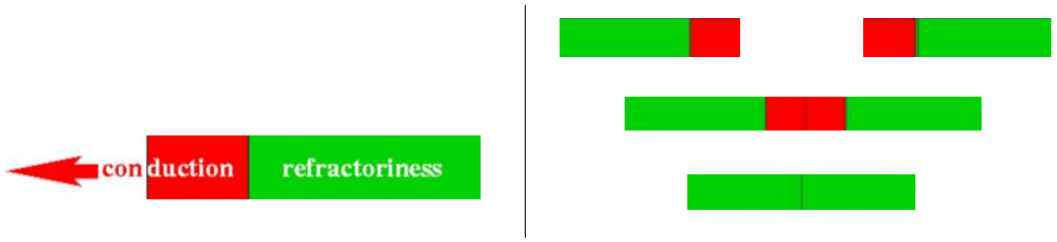


Figure 1.13: Left: Illustration of the refractory period after the passage of an exciting wavefront. Right: the annihilation of wavepropagation due to colliding fronts, from Waves and patterns in biophysics, A. Panfilov.

Wave-front annihilation

Characteristic for waves with a refractory period is the possibility to annihilate a wave with the help of another wave, moving towards the first one. When the wavefronts reach each other, they will trigger the medium to the excited state. As the medium around the wavefronts is already excited, the waves will annihilate. This is illustrated in Figure 1.13 on the right.

Competing sources

Within this context, it is more plausible to see why the SA-node in normal conditions is the pacemaker of the heart. The AP of the pacemaker cells in the SA-node, differ from the normal cardiac cells, as can be seen in Figure 1.14. The pacemakercells depolarize spontaneously at a rate of 70-80 times per minute. As the AP of a cardiac cell takes on average 300 ms, the cardiac tissue can sustain the waves created at the rate of the SA-node. Consider an ectopic pacemaker, which are spontaneously depolarizing cells at a slower discharging rate then the SA-nodal cells. If the sources start to pulsate and send out the electric signal, they both create concentric wave-fronts, which propagate further away. As the SA-node is able to give an electric pulse more fast, the wavefronts of the SA-node will always reach further than the fronts of the ectopic pacemaker. If we wait a while and let the two sources compete, the fronts of the SA-node will eventually reach the ectopic pacemaker, forcing the surrounding-tissues to excite at the phase determined by the SA-node, which thus determines the heart-rhythm. An illustration of two competing sources is shown in Figure 1.15.



Figure 1.14: The action potential of the pacemaker cells and normal cardiac cells.

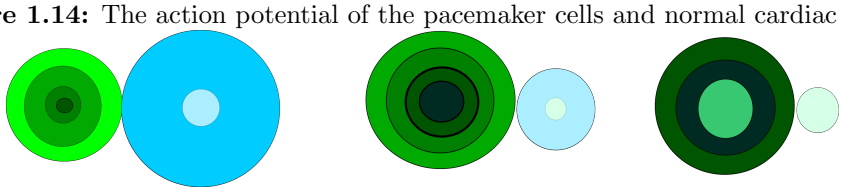


Figure 1.15: An illustration of competing spherical sources.

Spiral formation

Consider the ring-shaped tissue in Figure 1.16 a. This could be seen as an exciting wave, travelling around a very large obstacle. In case the refractory-period R, the circumference L and the speed of the wave v behave like Formula 1.15:

$$R < L/v \tag{1.15}$$

the tissue will be able to sustain the wave, and it will keep on circle around the obstacle. If we reduce the obstacle, the wavefront spans a larger area. If we consider the cells identical spread over the total tissue, they will pass the electrical impulse with the same speed. Therefore, at a larger radius from the heterogeneity, the wavefront will fall behind, creating a spiral-like pattern around the core. The possibility to sustain the spiral is determined by Formula 1.15 at the edge of the obstacle, thus if vR = L at the core.

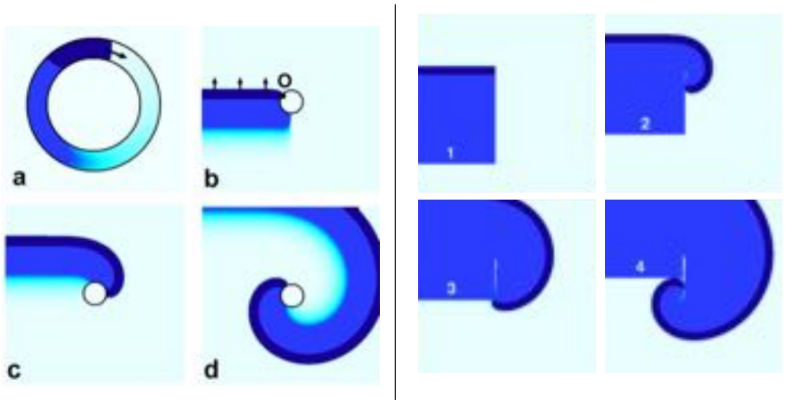


Figure 1.16: Spiralwave creation around and without an obstacle, resp. left and right, from Waves and patterns in biophysics, A. Panfilov.

In case there is not a heterogeneity, it is still possible for the wavefront to create a spiral. Considering the first graph in the right of Figure 1.16. Depending on where you are at the wavefront, the dynamics will be slightly different. At the edge of the tissue, the front is only responsible for the excitation of the heartcell in front of it. The wavefront in the middle can however excite multiple cells. The wavefront therefore curls at the middle, eventually resulting in a spiral.

7. The electrocardiogram ECG

When the excitation wave propagates through atria and ventricles, each cell undergoes an AP, passing the electrical impulse. The accumulation of the changing AP of all heartcells results in a contineously changing electrical field, changing both in direction and magnitude. This changing electrical field can be recorded on the chest with electrodes. The signal on the ECG thus is a projection of the changing electrical field on the surface of the heart. With knowledge of the signatures of a healty heart, the ECG is an easy and often used tool to determine the patient's heart condition.

Signature of the healty heart on ECG

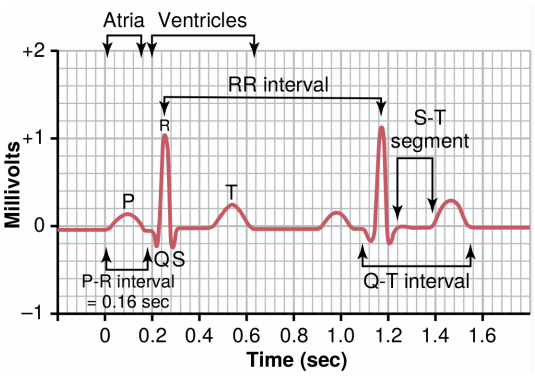


Figure 1.17: Illustration of the PQRST-signature, from Medical Physiology, Guyton and Hall.

Figure 1.17 shows the electrical recording of 2 heartbeats. Each normal heartbeat is marked with the PQRST-complex. A small P-wave, a QRS-peak and a T-wave. The P-wave is created by the depolarization of the atria. As the atria are small in comparison with the ventricles, this bump in the ECG is less pronounced then the QRS-peak and T-wave, created by the ventricles. There are less cells to depolarize, so a smaller electrical field is created. The preceding of this bump is a nice validation of the electrical decoupling of the atria and ventricles: the wave indeed needs time to pass the AV-node and reach the ventricles. In order

to understand the QRST-complex, we look at the typical form of the AP of the cardiac cell. The AP changes at first very fast due to the sodium-upstroke, resulting in the QRS-complex on the ECG. Afterwards, the cells undergo their plateau phase and altough there flow a lot of different ions through the membrane, the inward and outward currents compensate each other and the resulting electrical field is zero. Therefore, the signal on the ECG decreases. When the cells repolarize, the AP decrease to the resting potential state, changing the membrane potentials and thus the electrical field which emerges as the T-wave on the ECG. We illustrate the relation between the AP and the ECG in Figure 1.18.

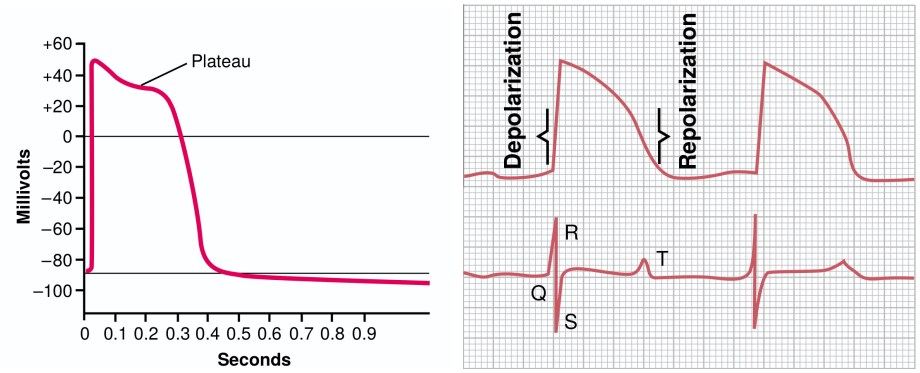


Figure 1.18: The AP of a single cardiac cell, left, and the creation of the PQRST-signature on cardiac level due to this AP, right, from Medical Physiology, Guyton and Hall

Signature of cardiac arrhythmias on ECG

From the moment the homogeneous spreading of the excitation wave is disturbed, due to spontaneous wave-break or heterogeneities in the tissue, this will lead to a certain effect visible on the ECG. Depending where the malfunctions appear and which effects they induce, different features will show on the recordings.

Ectopic beats Ectopic beats are the ones who are initiated by an ,,ectopic" pacemaker, which means ,,not the SA-node". Besides the fibers in the SA-node, the AV-nodal and Purkinje fibers are also able to discharge spontaneously but at a lower speed. The SA-nodes can discharge at a rate of 70 to 80 times per minute, in accordance with the mean human heart-rate, whilst AV-fibers respectively Purkinje fibers discharge at a rate of 40 to 60, respectively 15 to 40 times per minute. Hence, the SA-node will always be able to send out a new pulse, before the Purkinje or AV-nodal fibers were able to discharge spontaneously. Occasionally, it happens that AV or Purkinje-fibers do become excessively excitable (due to inflammation, viral infections or drugs intake, like caffein, temporarily malfunctions) and become a faster discharging source. In that case, an excitation wave will spread starting from the ectopic pacemaker, resulting in

an ectopic beat on the ECG. The ectopic beat can arise in the atria or the ventricles. They are called APC and VPC, Atrial resp. Ventrical Premature Contraction. The first graph of Figure 1.19 illustrates the VPC signature on the ECG.

Tachycardia When the excitation wave in the heart reaches a quasi-stable state, rotating around a point (around damaged tissue or spontaneous, see section 6) in a spiral-shaped form, large parts of tissue will be depolarized at a very high rate, determined by Formule 1.15. As the spiral is not able to homogeneously excite the heart, the pumping will become inefficient. This arrhythmia is called Tachycardia and can happen in both atria and ventricles. The severity of this excitation form in the atria is less endangering as the electrical impulse can still reach the AV-node were the normal healty bundle can pass the signal through the Purkinje network, exciting the ventricles and make them contract without knowledge of the disturbed pattern in the atria. The walls of the ventricles are large and strong enough to create suction after contraction and collect enough blood. If however the pattern arises in the ventricles, interference is needed. The second graph in Figure 1.19 shows an illustration of VT (ventricular tachycardia).

Fibrillation It's possible that the quasi-stable spiral loses it's stability and breaks up into countless smaller wavefronts, circulating on the tissue. This leads to a total breakdown of coordinated contraction. Atrial Fibrillation AF needs to be stopped because if the blood is held up in the atria due to the uncoordinated contractions, it is very likely it starts to create blood clots, which block the circulatory system inducing strokes. Ventricular Fibrillation needs to be stopped immedeatly as it is lethal in seconds to minutes. Figure 1.19 illustraties in the last 2 ECG the signature of AF and VF. Figure 1.20 shows a schematical representation of the excitation pattern, resulting in Tachycardia and Fibrillation.

Torsade de Pointes Torsade de Pointes (TdP, illustrated in Figure 1.21) is a form of polymorphic VT associated with a long QT interval on the resting ECG. During Torsades de Pointes the ventricles depolarize in a circular fashion, resulting in a characteristic illusion of a twisting of the QRS complex around the isoelectric baseline of the ECG. The mechanisms underlying this cardiac arrhythmia remain still poorly understood. Thanks to the collaboration with the research group of Professor Seemann from Freiburg, we will be able to create ECGs of the excitation patterns we induce. We will compare the resulting ECGs with those of TdP.

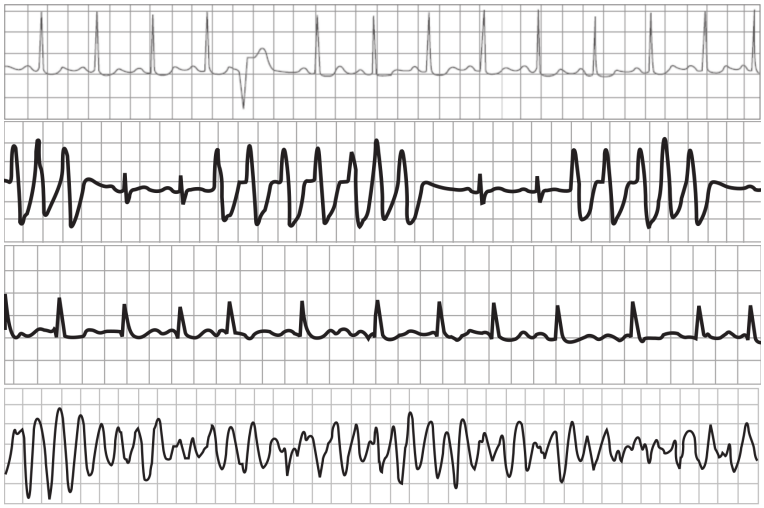


Figure 1.19: From top to bottom, illustration of the ECG of a ventricular ectopic beat VPC, Ventricular Tachycardia VT, Atrial Fibrillation AF and Ventricular Fibrillation VF, from Advanced methods and tools for ECG data analysis, Andrew T. Reisner, Gari D. Clifford, and Roger G. Mark.

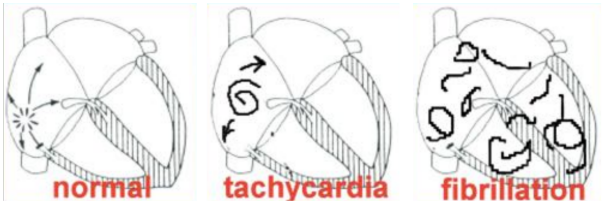


Figure 1.20: Schematical representation of the excitation patterns causing arrhythmias, from Waves and patterns in biophysics, A. panfilov.

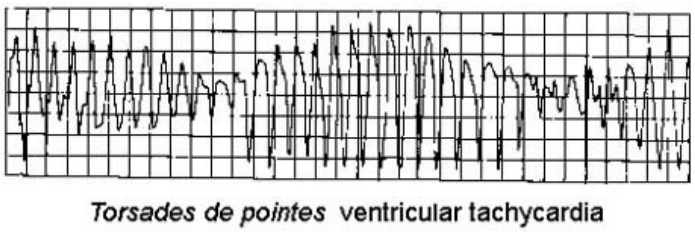


Figure 1.21: Illustration of TdP on the ECG.

Chapter 2

EAD-induced patterns in 2D

The aim of this thesis is to perform a systematic study of EAD-induced pattern formation in a 3D model of human ventrical tissue. For this study, the methods and techniques of the paper ,,A study of EAD in an anatomically correct model of the human ventricles in 2D [8]" will be used. As said in section 5 of previous chapter, an EAD is a depolarization during the repolarizing phase of the AP. In Vandersickel et al. [8], the results of an extensive numerical study are presented. This study focussed on the influence of EADs on wave-break and the resulting pattern-formation in a 2D tissue model of human ventrical cells. For this, the TNNP-TP06 model for human ventricular tissue was used (see section 3 of previous chapter [6, 7]). At first, the conditions responsible for the onset of EADs at the single-cell level were studied. Based on experimental results which have been shown to evoke EADs at this level, this was done by increasing I_{Ca_L} and decreasing I_{KR}. Afterwards, a 2D sheet of ventrical tissue was used to study how EADs at single cell level could result in fibrillation at tissue level. Gradually lowering the I_{KR} and raising the I_{Ca_L} resulted in the classification of three different patterns which emerged in the mathematical sheet of human ventrical tissue. The three patterns were called spiral fibrillation type b SFb, spiral fibrillation type a SFa and Oscillatory type Osc.

1. SFb, SFa and Osc: 3 wave patterns due to EADs

To induce the patterns in the tissue sheet of cardiac cells in [8] 2 protocols were used. For the first protocol, a small rectangular region at the edge of the sheet was stimulated: the S1-pulse. For the second protocol, a spiral with the standard S1S2 stimulation protocol was induced [35]. Hereby, the left side of the tissue is stimulated to induce a plane wave propagating from the left to the right side of the tissue. When passed over the first half of the stimulation domain, a second smaller stimulus over the first quarter of the domain is applied, resulting in the spiral wave. Starting from this stable spiral, the parameter values were gradually changed by lowering I_{KR} and raising I_{Ca_L}. For the first protocol, the S1-pulse

is applied in a homogeneous tissue-sheet at resting potential for different parameter values. We represented the used protocols in Figure 2.1.

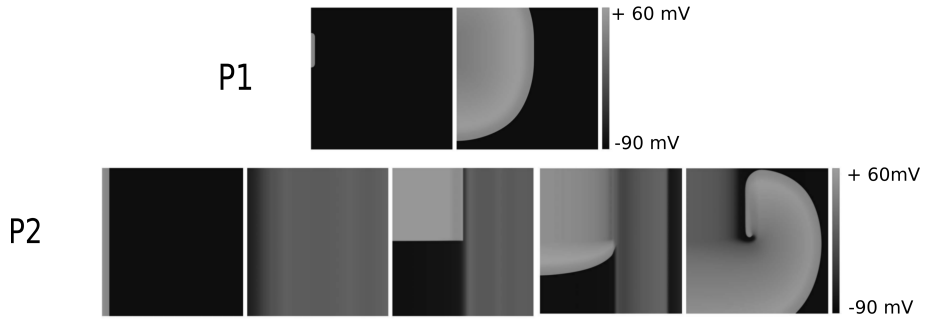


Figure 2.1: The used protocols P1 and P2 for the study of EAD in 2D from [8].

As mentioned before, 3 types of patterns emerged in different parameter regions. The results are illustrated in Figure 2.2. The background color illustrate the behaviour at single cell level. The yellow region denotes normal AP. The red region denotes AP with EADs but repolarization still emerges. The blue region denotes the parameter region where the single cell fails to repolarize and where the AP is bounded by a certain amplitude.

The SFb-type pattern

The SFb type pattern emerges due to wave-break at the center of the spiral created with the second protocol. It was not possible to create this pattern with the first protocol. The SFb pattern is a complex-spatio temporal pattern of waves alterning the tissue from a repolarized to a depolarized state. We clearly see in Figure 2.3 regions of complete repolarization, indicated by the black regions, next to depolarized regions.

The SFa-type pattern

The SFa type pattern consists of multiple interacting spiral waves. These spiral waves occur due to wave-breaks of the applied stimuli. An example of the voltage excitation pattern of the SFa type is shown in Figure 2.3. An important note is that it becomes increasingly harder for the cells in the SFa pattern to repolarize completely when I_{Ca_L} is raised deeper in the red region of Figure 2.2. This shows in the voltage-pattern by the fact that there are no clear dark regions which separates the waves, indicating a smaller amplitude in the AP of the cells.

The Osc-type pattern

The patterns in the oscillatory regime can have various unusual manifestations, running from point sources to lines of point sources. Most importantly, the patterns all have an oscillatory underlying dynamic. Its clear from Figure 2.3 that the cells do not repolarize anymore in the oscillatory regime.

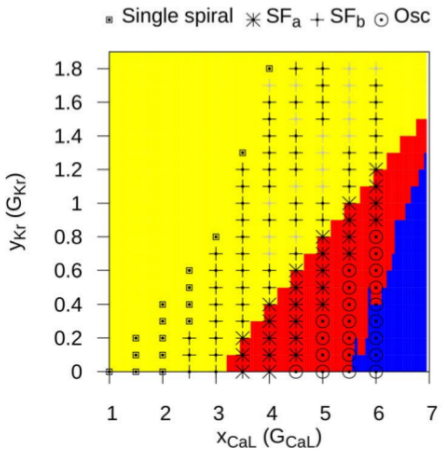


Figure 2.2: Parametric space of EADs induced spatial patterns SFb, SFa and Osc Illustration of the 2D parameter space in which the different types of patterns emerged. [8]

2. Calcium and sodium mediated waves

Also illustrated in Figure 2.3 is the opening and closing of the L-type calcium gates (given in equation 1.12 of section 4, previous chapter) and the opening of the sodium gates (given by equation 1.14 of section 4, previous chapter). With increasing I_{Ca_L} the sodium mediated waves disappeared and the pattern emerged due to calcium mediated waves. We see that the SFb type pattern is determined by both, whilst the SFa type mostly and Osc type only emerge from the calcium waves.

3. Phase waves vs real waves

Real waves are understood as electrical-activation gates, resulting from the interplay between the excitability of the cell in the tissue sheet and the diffusion between those cells. They travel with a velocity proportional to the square root of the diffusion coefficient. Phase waves however are waves without interaction. The pattern emerges from a shifted phase between neighbouring oscillators: the cells in the oscillatory regime. They placed barriers in the tissue sheet by mathematically decoupling the tissue along an orthogonal grid. The barriers are impermeable. The SFa- and SFb-type disappear after the barrier is imposed which illustrates

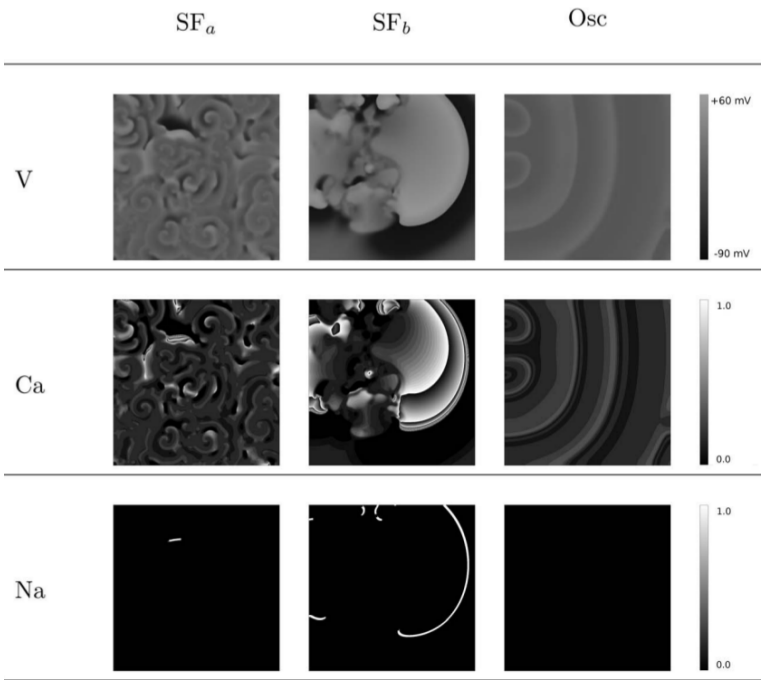


Figure 2.3: The SFa, SFb and Osc -type Illustration of the voltage patterns, the output of the Calcium gates and the output of the sodium gates from [8]

their real-wave nature. The Osc-type patterns however are not affected by the barriers and the waves seem to propagate through the barriers.

4. ECG and Fouriertransforms

From each pattern, an ECG and the average fourier transform of 10.000 points equally distributed over the tissue-sheet was calculated (Figure 2.5). The fourier transform and ECG represent 1D information of the 2D tissue consisting 1000 x 1000 cells. The temporal fourier transform of the voltage shows the fundamental peaks of each pattern. For example the peak at 6 Hz of the Osc type fourier transform is equal to the inverse of the average distance between 2 small peaks in the APs of the cells. For the oscillatory pattern a stable periodic ECG is visible.

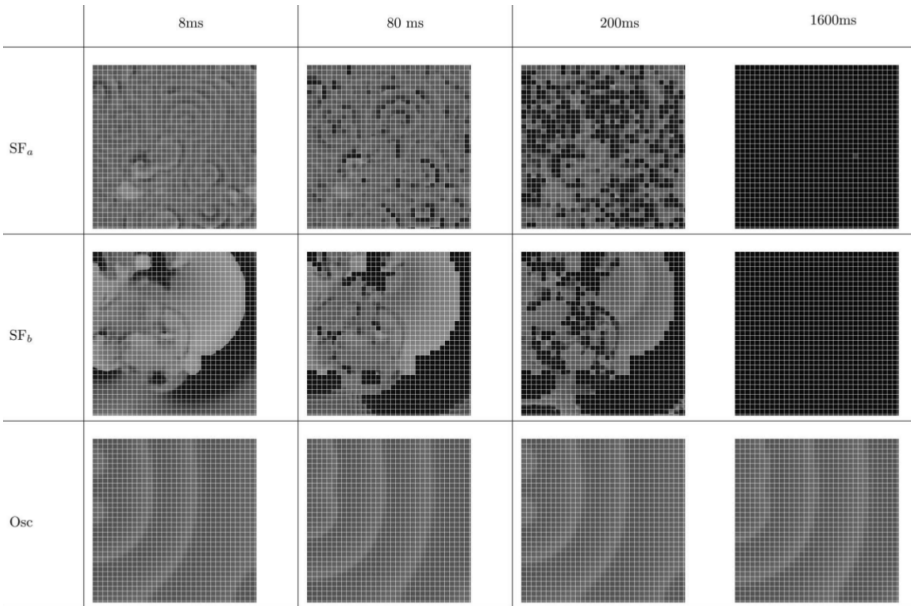


Figure 2.4: Phase waves vs real waves Illustration of the grid-shaped decoupling of the tissue-sheet where the Osc type move undisturbed through the unpermeable walls, whilst the SFa and SFb type clearly are hinderded by the decoupling, from [8]

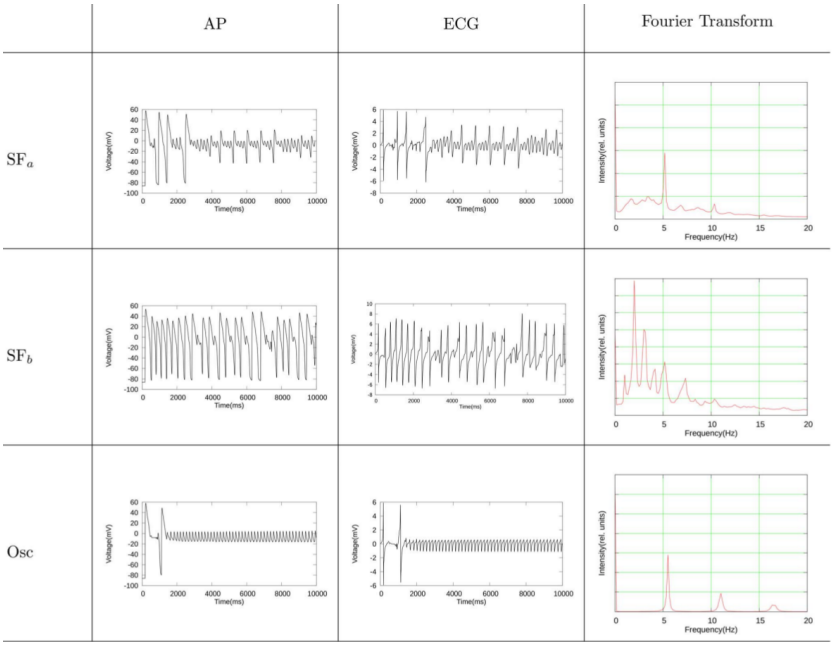


Figure 2.5: Time course characteristics Illustration of AP, the ECG and the temporal fourier transform of the 3 types, from [8]

Chapter 3

EAD-induced patterns in 3D

During this thesis, we performed a systematic study of EAD pattern formation in a 3D model of the human ventricles. For this, we used the TNNP-TP06 mathematical model for human ventrical cells [6,7] and -unless otherwise specified- we used the default parameters. An overall modification, as in [8], is the twofold decrease of the time constant τ_f of the f-inactivating gate of the L-type calcium current (see equation 1.12 from section 4, chapter 1), in order to induce the EADs. As this results in shortening of the AP, we have increased the value of G_{Ca_L} by a factor of 2. This modified version of the TNNP-TP06 model gives almost the same representation of the restitution properties of the cell as in the original model [6,7]. The dynamics of each individual current is given by an ODE system with 18 state variables. All our simulations have been carried out in an isotropic domain with a diffusion constant D = 0.00154 cm^2/ms, with a time step of 0.02 ms and a space step of 0.25 mm in the 3 orthogonal directions. A uniform grid of dimensions 345 x 244 x 268 was used. We multiplied the individual gridpoints with a factor 0 or 1 denoting a void or a heartpoint in order to create the anatomical shape of the heart. For the whole heart simulations an explicit first order Euler method is used to solve the discretized system. To integrate the HH-type equations for the gating variables of the various time-dependent currents the Rush and Larsen scheme is used [36]. Thanks to the highly parallel code, implemented on GPUs, created by the research group of Professor Panfilov, we were able to do high speed computations, with a minimum of resources.

1. Methods

In order to induce EADs, the repolarization reserve RR should be reduced [14–16]. This can be done by decreasing outward currents like I_{KR}, I_{KS} or increase inward currents like I_{Ca_L}. We have followed the approach of [8] and studied the EADs by gradually changing I_{KR} and I_{Ca_L}. Similar to [8], 2 protocols to induce the EADs were used: the S1 pacing and S1S2-protocol. For both protocols, an S1-pulse on the heart was applied by setting the voltage to

+50 mV in a certain region as shown in Figure 3.1.

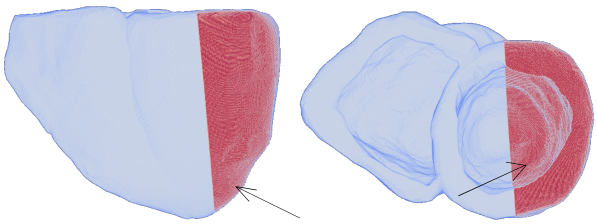


Figure 3.1: Illustration of the S1-pulse.

S1 pacing

For the S1 pacing protocol each time the voltage in the point, marked with an arrow in Figure 3.1, was below -60 mV a new S1-pulse was applied. The number of pacings was set to 10 times. In a few cases, the cells failed to repolarize after the first applied pulse. Therefore, the threshold value was not reached and we paced only once. The parameter region of 10 S1-pulses is shown in Figure 3.2 in red. The parameter values for which we only paced once are shown in yellow. The probed parameter region is determined by a 6- to 15-fold of the default value of I_{Ca_L} and a 0.0- to a 1.5-fold of the default value of I_{KR}. We simulated 4000 ms in which the pulses were applied. Afterwards another 2048 ms were simulated to let the patterns evolve.

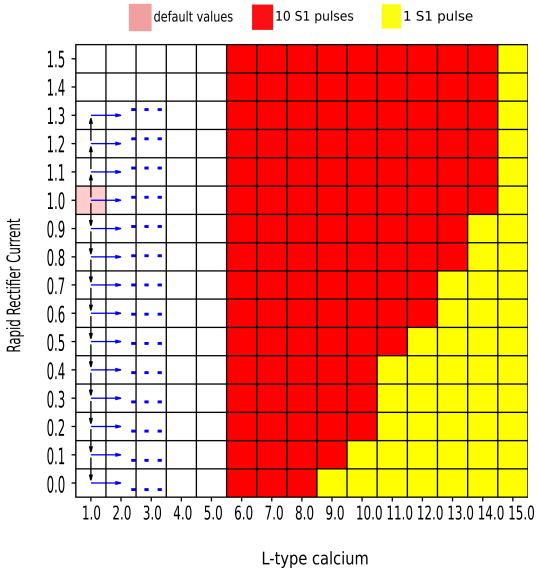


Figure 3.2: Parameter range for the S1 pacing and S1S2 protocol. We illustrated the probed parameter range for both protocols. S1S2: The pink square represents the default values of the TNNP-TP06 model, whereby the stable spiral was created. Starting from here, we lowered and raised I_{KR} until the spiral settled. We then followed the blue arrows by raising I_{Ca_L} gradually until the pattern stabilized in the new parameter region. S1 pacing: The parameter ranges for 10 S1 pulses is shown in red. Parameter values for which we paced only once are denoted in yellow.

S1S2

For the S1S2 protocol, the S2-pulse was applied after the first S1-pulse, consequently resulting in the stable spiral shown in Figure 3.3. We probed a range by a 1- to 15-fold of the default value of I_{Ca_L} and a 0.0 to 1.3-fold of the default value of I_{KR}, as shown in Figure 3.2. The pink square represents the default values for which the single stable spiral SSS was created. Then, we lowered and raised the I_{KR} value gradually as shown by the black up and down arrows, until the spiral stabilized in the new parameter region. We simulated 1500 ms of each stable spiral of the different I_{KR}-values. Starting from these spirals the I_{Ca_L} value was gradually raised, as shown with the blue arrows in Figure 3.2. Depending on the stability of the excitation pattern in the new parameter region, the simulations took from 1500 up to 3000 ms. We illustrated detailed in Tabel 3.1 the simulation time of each increasing step of I_{Ca_L}.

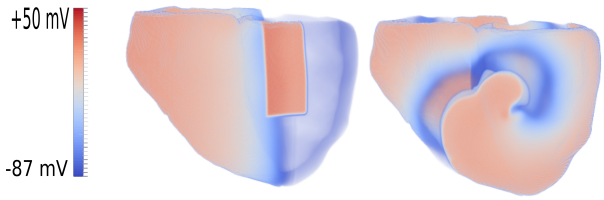


Figure 3.3: Creation of the single stable spiral at the default parameters with the S1S2-protocol. At the left: the S2 pulse after the passing of the S1 pulse from Figure 3.1. At the right: the resulting stable spiral at the default values.

ECG creation

Thanks to the collaboration with the research group of Professor Gunnar Seemann, we have the software available to create the ECGs of our mathematical heart-model. In general, an ECG is created by applying electrodes on the chest, recording the changing electrical field due to the AP, as explained in section 7 of chapter 1. Combination of the records from certain reference points results in the ECGs. An illustration of the different applied electrodes in the software of Professor Seemann is illustrated in Figure 3.4. With this software, we calculated the ECGs of the voltage-patterns and we compared them to clinical ECGs of TdP.

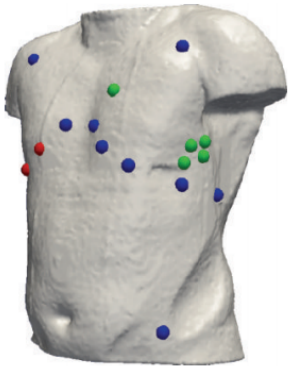


Figure 3.4: Torso with the applied electrodes. Blue electrodes are needed for the collection of ECGs used during this thesis, from [31].

	Applied simulation time in ms for the S1S2 protocol				
I_{Ca_L}	$I_{KR} = 0.0$	$I_{KR} = 0.1$	$I_{KR} = 0.2$	$I_{KR} = 0.5$	$I_{KR} = 0.6$
1.0	1500	1500	1500	1500	1500
2.0	1500	1500	2000	2000	2000
3.0	1500	1500	2000	2000	2000
3.2	1500	3000	2000	2000	2000
3.4	1500	3000	2000	2000	2000
3.6	1500	3000	2000	2000	2000
3.8	1500	3000	2000	2000	2000
4.0	1500	3000	2000	2000	2000
4.1		3000			
4.2	1500	3000	3000	2000	3000
4.3		3000			
4.4	1500	3000	3000	2000	3000
4.5		3000		2000	
4.6	1500	3000	3000	2000	3000
4.7		3000	3000	2000	
4.8	1500	3000	3000	2000	3000
4.9		3000	3000	2000	3000
5.0	1500	3000	3000	3000	3000
5.1	3000	3000	3000	3000	3000
5.2	3000	3000	3000	3000	3000
5.3	3000	3000	3000	3000	3000
5.4	3000	3000	3000	3000	3000
5.5	3000	3000	3000	3000	3000
5.6	3000	3000	3000	3000	3000
5.7	3000	3000		3000	
5.8	3000	3000	3000	3000	3000
5.9	3000				
6.0	3000	3000	3000	3000	3000
6.1				3000	
6.2				3000	3000
6.3				3000	
6.4				3000	3000
6.5				3000	
6.6				3000	3000
6.7				3000	
6.8				3000	3000
6.9				3000	
7.0 to 15.0	3000	3000	3000	3000	3000

Table 3.1: Applied simulationtime for each parameter value probed with the S1S2-protcol.

2. Results of the S1S2 and S1 pacing protocol

The S1 pacing protocol resulted in three different types of excitation patterns: SFb, SFa and Osc. These patterns are similar as observed in [8]. With the S1S2 protocol we found the same three patterns for the same parameter values. In addition, we consequently saw the spiral meandering in the parameter range close to SFb. Figure 3.5 combines the results of the S1S2 and the S1 pacing protocol. We showed the parameter range in which a certain pattern arose. Due to the extensive computational cost of the S1S2 protocol a smaller range was probed. We note that if for a certain parameter range both protocols resulted in pattern formation, we compared the final patterns and found that they did not depend sensitively on the initial conditions. Below we described extensively the features of the three patterns. Afterwards, we discussed the meandering spiral and its characteristics on the ECG.

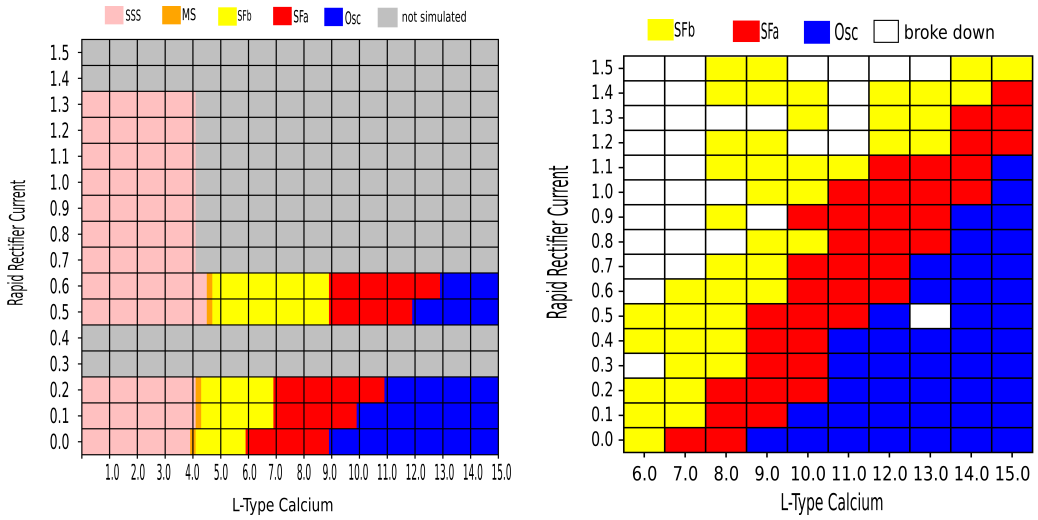


Figure 3.5: Classification of the 5 different type of patterns with the S1S2 protocol (left) and with the S1 pacing protocol (right). We denoted the range of the single stable spiral SSS, the meandering spiral MS and the three patterns SFb, SFa and Osc.

3. The SFb, SFa and Osc-type patterns

A. Pattern description of SFb, SFa and Osc

SFb The SFb-type pattern is a complex spatio-temporal pattern at the large-scale of the heart. The heart is in a chaotic bi-stable regime mediated by sodium and calcium waves. We saw regions of complete repolarization alternating with depolarized regions, which resulted in the large amplitude of the AP of each cell. We illustrated in Figure 3.6 the evolution of the SFb pattern starting from the S1 pacing protocol. The parameter values are $I_{KR} = 0.6$ and $I_{Ca_L} = 8.0$.

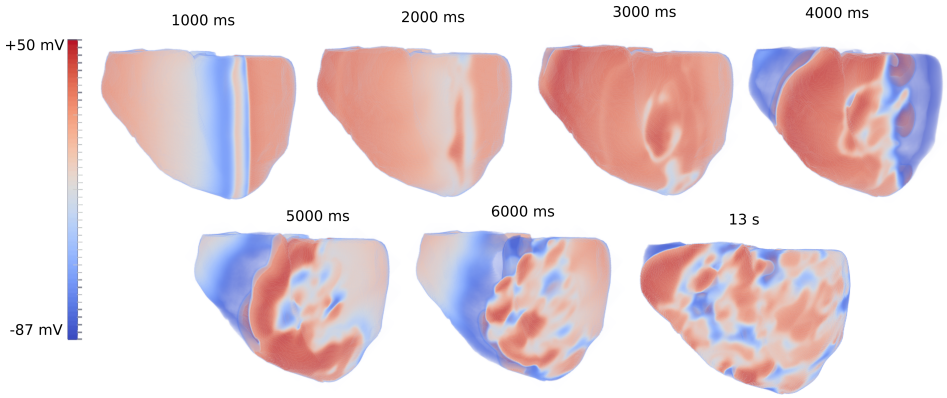


Figure 3.6: SFb pattern Evolution of the SFb pattern with the S1 pacing protocol for $I_{KR} = 0.6$ and $I_{Ca_L} = 8.0$ times the default values.

SFa We illustrate the SFa pattern formation in Figure 3.7 for $I_{KR} = 0.6$ and $I_{Ca_L} = 11.0$. We see in the Figure that the excitation pattern evolves to a state of multiple small rotating spirals. Those spiral waves are the result of multiple wave breaks. Even if the first break appears in a complete different region of the heart, the final state for all patterns in the category of SFa are similar. The resulting spatio-temporal patterns are rather complex. Between the waves and spirals, the heart-tissue does not repolarize completely. We see this by noting that the intermediate tissue in the excitation pattern of SFa is not dark blue, in contrast with the blue regions of the SFb patterns. Compared to SFb, the cells fail to repolarize to the resting potential state at -87 mV.

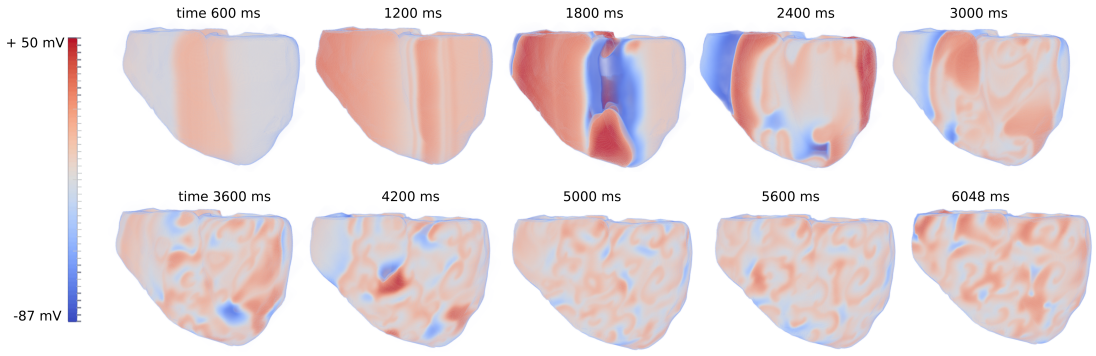


Figure 3.7: SFa pattern Evolution of the SFa pattern with the S1 pacing protocol for $I_{KR} = 0.6$ and $I_{Ca_L} = 11.0$ times the default values.

Osc We illustrate typical Osc patterns for $I_{KR} = 0.6$ and $I_{Ca_L} = 13.0$ for both protocols in Figure 3.8. In the parameter region where the Osc patterns emerge, the individual cells

can not repolarize. Therefore, the AP of the cells oscillates and has a small amplitude. This is in contrast to the alternating AP of the SFb and SFa patterns. The final state of the Osc patterns differed depending on the inital pulse. For the S1 pacing protocol, it looks as if the S1-pulse is still applied. This is not the case as the cell does not reach the threshold for stimilus. For the S1S2 protocol, it seems as if the spirals of the SFa type pattern disappear due to diffusion into an smoother excitation pattern.

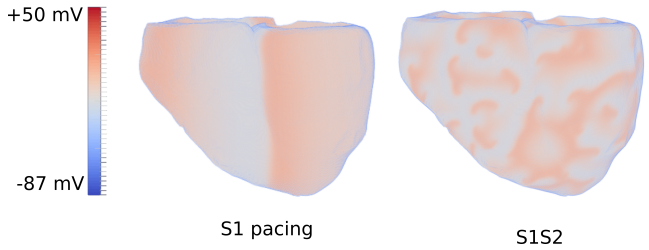


Figure 3.8: Osc pattern Illustration of the Osc pattern for both the S1 pacing as the S1S2 protocol. We saw a difference due to the differing initial applied pulse.

Note: cross-section Figure 3.9 illustrates both endocardial and epicardial view of the heart. We see similar evolved excitation patterns at both sides of the tissue.

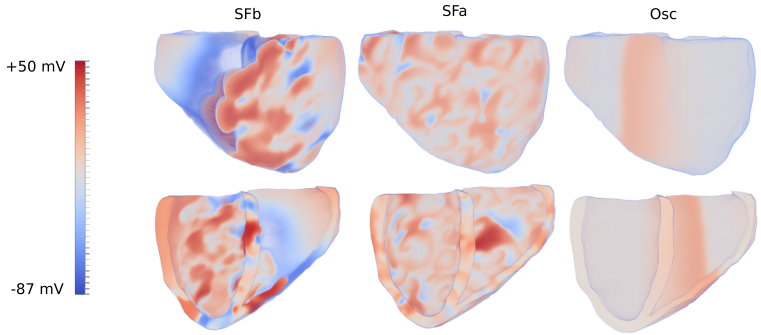


Figure 3.9: Cross-section of the heart Cross-section of the excitation pattern in the heart for the three patterns for $I_{KR} = 0.6$ and $I_{Ca_L} = 8.0$, 11.0 and 13.0 times the default.

B. AP profiles

The typical APs of the SFb, SFa and Osc type are represented in Figure 3.10. We showed the APs of the stepwise increase of I_{Ca_L} from 7.0 to 15.0 times the default value. The value of I_{KR} was set to 0.6 times the default value. Further, we will see that mechanisms of pattern formation are initially located at the edge of the applied S1 pulse. Therefore pattern formation was more developed in this part of the tissue. We recorded the AP of heartcells in regions where the pattern was developed.

SFb In the first column the APs of three SFb patterns for I_{Ca_L} equal to 7.0, 8.0 and 9.0 are shown. The cells clearly repolarize, even after multiple small EADs. When I_{Ca_L} is increased, the amplitude of the EADs becomes increasingly larger, but the resting potential necessary for I_{Na} recovery is still reached.

SFa The second column of Figure 3.10 shows three APs of the SFa patterns for I_{Ca_L} equal to 10.0, 11.0 and 12.0. By increasing I_{Ca_L} repolarization after multiple EADs becomes unlikely. The reducing amplitude of the APs is in accordance with the light blue regions of the excitation patterns. Typical for SFa as in 2D [8] is the emergence of alternating EADs. We can see a slightly larger amplitude alternating with smaller bumps in the AP.

Osc The cells were in an oscillatory regime and the amplitude of the AP stayed very small. The last column of Figure 3.10 illustrated the AP of three Osc patterns for I_{Ca_L} ranging from 13.0 to 15.0.

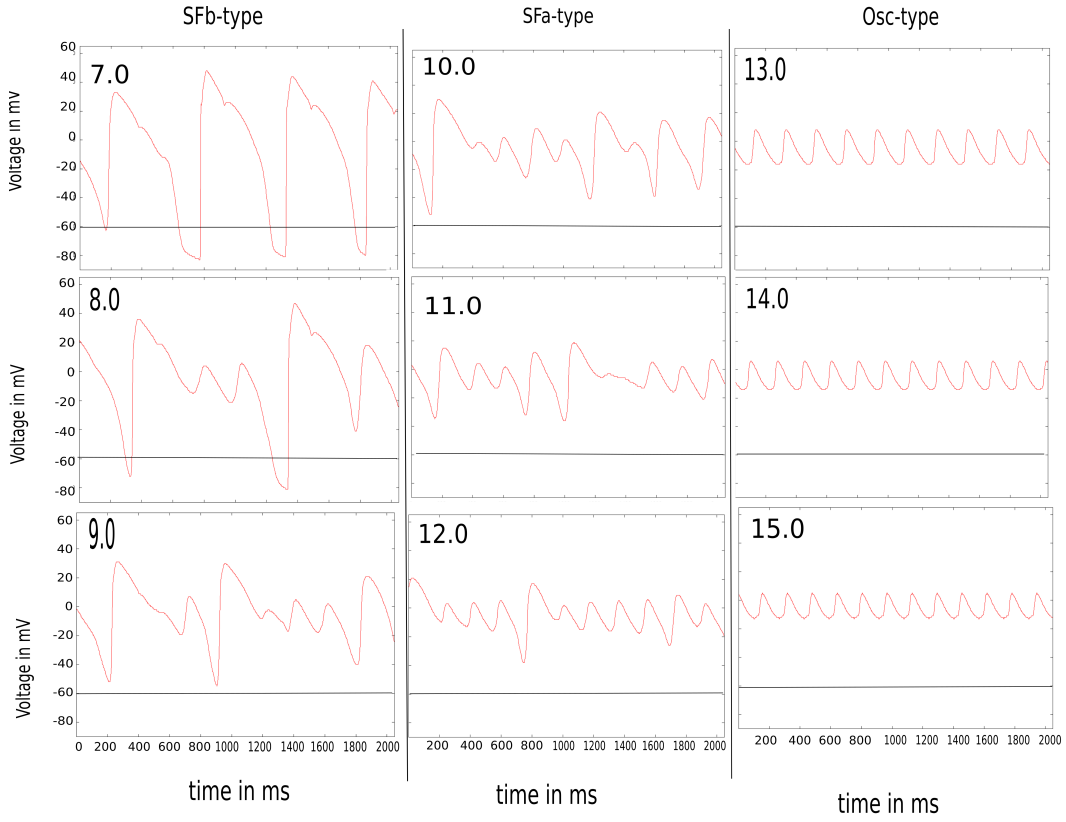


Figure 3.10: Typical AP for SFb, SFa and Osc In this figure we illustrated the typical AP of the three patterns. We saw a gradual transition from SFb to SFa into Osc by the decrease of the amplitude through the APs.

C. Mechanisms of pattern formation

SFb, SFa and Osc with S1S2 Starting from the meandering spiral with $I_{KR} = 0.0$ and $I_{Ca_L} = 4.0$, we further increased I_{Ca_L} gradually in steps of 0.2. With each step, we observed an increment in the complexity of the spatio-temporal excitation patterns, visualized in Figure 3.11. Initially at $I_{Ca_L} = 4.0$, we see the spiral meander. Increase to $I_{Ca_L} = 4.2$ resulted in the formation of two spirals and a backwards moving wave. Further increase resulted in an increase of the amount of spirals and eventually at $I_{Ca_L} = 5.0$ we see the typical SFb pattern. Starting from $I_{Ca_L} = 5.0$, we further increased to $I_{Ca_L} = 15.0$ and we observed a gradual change from SFb (at $I_{Ca_L} = 5.0, 6.0$) into SFa (at $I_{Ca_L} = 7.0, 8.0, 9.0$) into Osc (at $I_{Ca_L} =$ 10.0 - 15.0) which we illustrated in Figure 3.12.

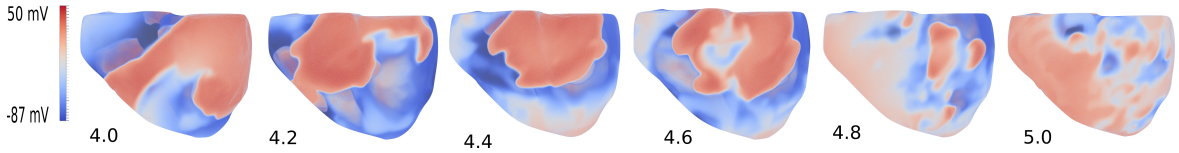


Figure 3.11: Increment of the complexity of the spatio-temporal pattern We show the increase of the I_{Ca_L} from 4.0 to 5.0 in steps of 0.2. The meandering spiral breaks up gradually and eventually results into an SFb pattern.

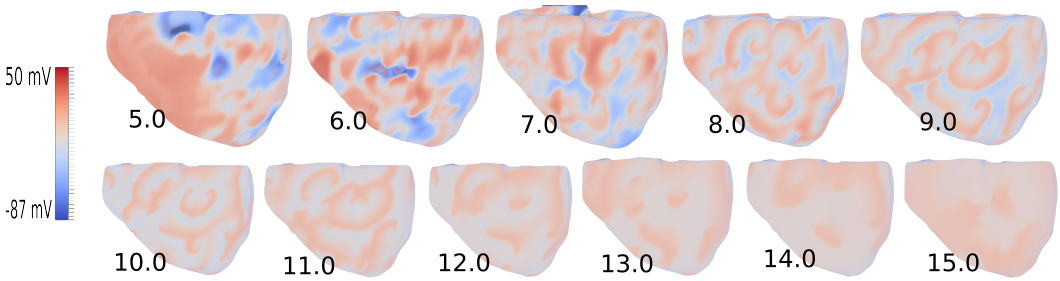


Figure 3.12: Transition from the SFb to the Osc exciation pattern We illustrate the step-by-step increase of I_{Ca_L} and the corresponding excitation pattern, contineously changing from SFb into SFa to Osc. The number denotes I_{Ca_L}.

We investigated the origin of spiral breakup for $I_{Ca_L} = 4.2$. In Figure 3.13, we marked the region of interest with a square. After 20-40 ms simulation time, a secondary excitation wave at back of the propagating spiral occurs and collides with the front of the spiral. At the same time in another place of the heart, another backwards propagation takes place (Figure 3.14). At t = 40 ms we clearly see a region of EADs emerging in the excitation pattern. To illustrate this, we draw the AP of the point marked with the arrow. EADs are clearly visible in this AP. Due to the emergence of the EADs, the complexity at the core is raised. The

EADs form an island which result in the creation of a new backwards propagating wave. This eventually results in the creation of 2 spirals (t = 400 ms). For the probed region of the S1S2 protocol, we observed similar scenarios where complex interactions of propagating waves with additional waves created by EADs resulted in new wave break formation.

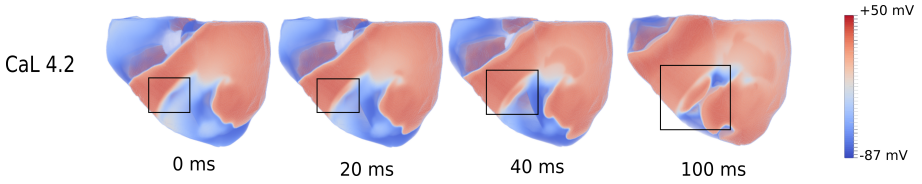


Figure 3.13: Backwards moving wave An illustration of a backwards moving wave.

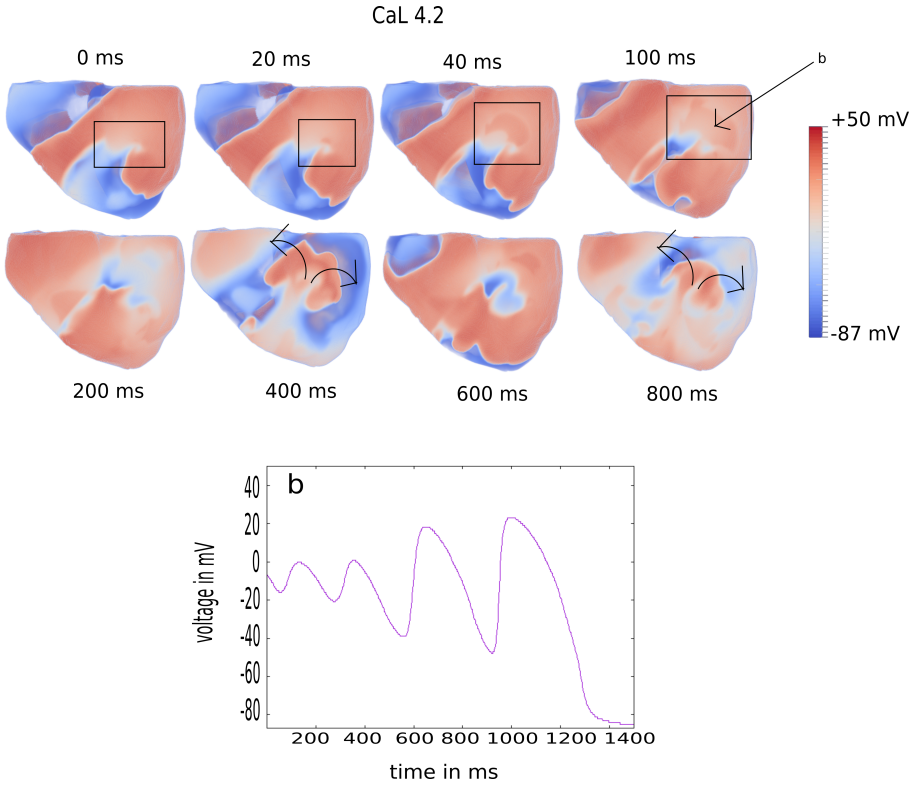


Figure 3.14: EADs at the meandering core We illustrate the raised complexity at the core due the EADs breaking the excitation pattern into 2 spirals.

We further consider the mechanisms of pattern formation for the S1 pacing protocol.

SFb, SFa and Osc with S1 pacing We illustrate the pattern formation for SFb in Figure 3.15 for $I_{KR} = 0.6$ and $I_{Ca_L} = 8.0$. After the 4th applied S1 pulse, we see multiple EAD regions at the back of the propagating wave. The AP of cardiac cells in this island shows EADs with large amplitudes. The timeshot at t = 2120 ms is shown and is denoted with the

vertical line in the graph. Previous small EADs, e.g. at t = 1250 ms did not form such EAD islands. As in the case of the S1S2 protocol waves starting from the EAD islands formed new spirals leading to the SFb pattern.

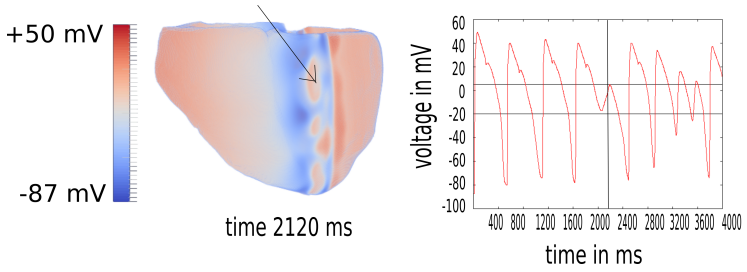


Figure 3.15: S1 pacing: EADs creating the SFb-pattern We illustrated the heart between the 4th and 5th S1pulse after 2120 ms simulation time. The graph illustrates the AP of the cell marked with the arrow.

The formation of the SFa pattern is illustrated in Figure 3.16 for $I_{KR} = 0.6$ and $I_{Ca_L} = 11.0$. Again, we see formation of EAD islands at the back of the propagating wave. Graph a illustrates the AP of a point in an EAD islands were EADs are clearly visible in the AP. Intrestingly enough the formation of the SFa pattern here is gradual. It is first formed at the left side of the heart were the tissue is paced intensively. Then it slowly spreads to the rest of the cardiac tissue. As in SFb, not every EAD resulted in wave break. In graph b we see the S1 pulses with a normal repolarization phase and small EADs which do not form new spirals. Only after the pattern was completely spread over the heart, these points started to show EADs with failing repolarization in the AP.

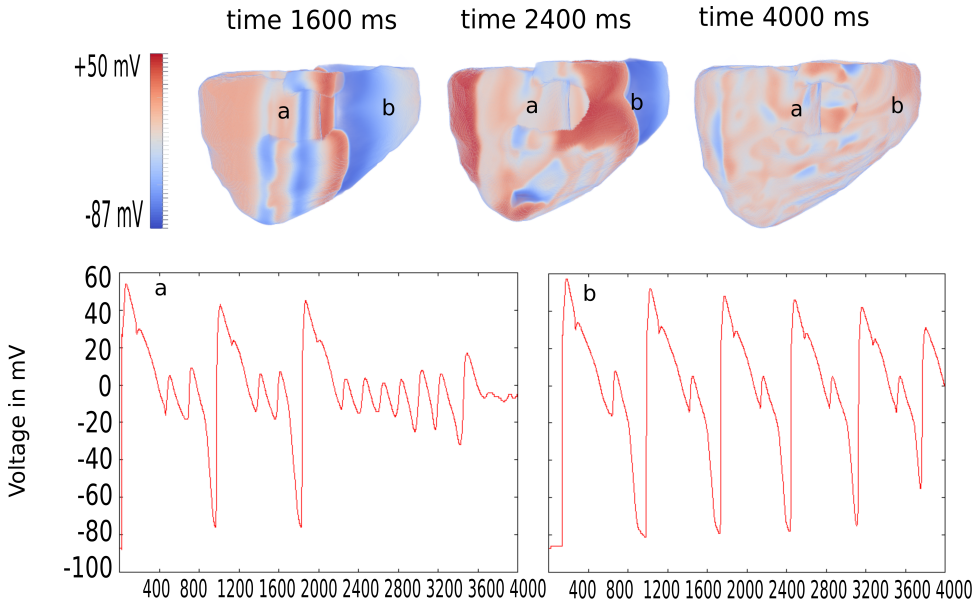


Figure 3.16: SFa pattern induced by EADs We illustrated timeshots after 1600, 2400 and 4000 ms. We show the AP of the points in a and b.

At least, we show the formation of the Osc pattern in Figure 3.17 for $I_{KR} = 0.6$ and $I_{Ca_L} = 13.0$. After the passing of the first S1 pulse, the cells fail to repolarize and they follow an oscillatory regime. The AP fluctuates with a small amplitude between -20 and 10 mV. The excitation pattern in the heart follows the form of the S1 pulse repeatedly as explained before.

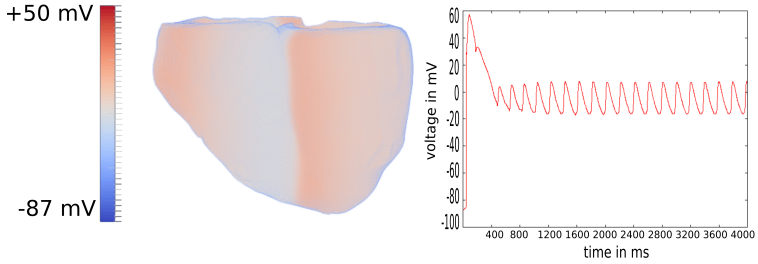


Figure 3.17: S1 pacing in the oscillatory region After applying the first S1-pulse, the cells failed to repolarize and followed an oscillatory regime.

D. Sodium and L-type calcium mediated waves

In normal conditions, excitation waves in cardiac tissue are driven by sodium currents. However, it is possible that the waves are mediated by calcium [37]. We studied the type of waves by plotting the activating and inactivating gates for either L-type calcium (simulation output

of given by $df f_2 f_{cass}$) and sodium (determined by the product m^3hj). The results are shown in Figure 3.18. We see as in 2D [8], that SFb is determined by both sodium and calcium waves whilst SFa is mainly determined by calcium waves. The Osc-type patterns are solely mediated by calcium waves. Note, that although in the case of SFb, only a small part of the tissue shows presence of sodium, this however changes in the course of time, and eventually, sodium is active in all heartpoints.

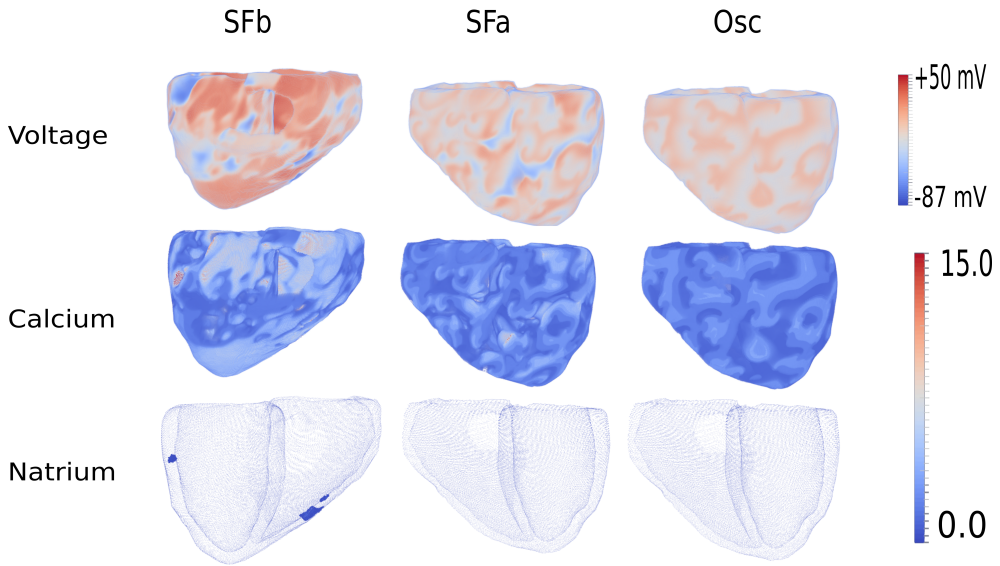


Figure 3.18: Sodium and calcium mediated waves On the final states of the S1S2 protocol we simulated another 1000 ms. We illustrated the opening and closing gates of L-type calcium and sodium and the voltage excitation pattern. The scale of the sodium and calcium-output is relative in order to produce the clearest images.

E. Statistical approach of the AP

As showed in Figure 3.10, the main difference between the SFb and SFa patterns is the ability of the AP (for the SFb type) to repolarize below -60 mV to allow I_{Na} to recover. Therefore the quantify this change from SFb to SFa patterns we developed the following procedure. We counted how often the AP passed the voltage-line of -60 mV and represented the results in Figure 3.19. These results are created during the simulations of 2048 ms of the S1 pacing data and are made with the following protocol. We took 3016 equidistant points in the heart which are the gridpoints of an equidistant orthogonal grid with an interspacing of 10 heartpoints. Of these heartpoints, we counted the amount of times the voltage was equal to (-60 $\pm$ 1) mV. Afterwards the result was devided by 2 to take into account the upstroke and downstroke of one AP and devided by 3016 to find the average amount of AP a cell undergoes during the simulation time of 2048 ms, hereafter called η. This resulted for our simulation time in η between 0 and 4. For example, for $I_{KR} = 0.6$ and $I_{Ca_L} = 7.0$ we found $\eta = 3.6$ which is

in accordance with graph a of Figure 3.10. We see that during this time interval, the AP reached the -60 threshold 3 to 4 times (depending on the heartpoint). For clearity we marked in Figure 3.10 -60 mV with a line. Another observation which we can make from Figure 3.10 is that the number of repolarizations below -60 mV decreased with increasingly I_{Ca_L}. The overall data for the parameter range determined by I_{KR} and I_{Ca_L} shows a gradually change of SFb to SFa. The decreasing value of η is in correspondence with the single cell behaviour and the excitation patterns we have been studying. For the S1S2 data we found likewise results, represented in Figure 3.20. The simulations here took 1500 ms to 3000 ms so we multiplied the resulting average with a factor to scale to the 2048 ms of the S1 pacing data.

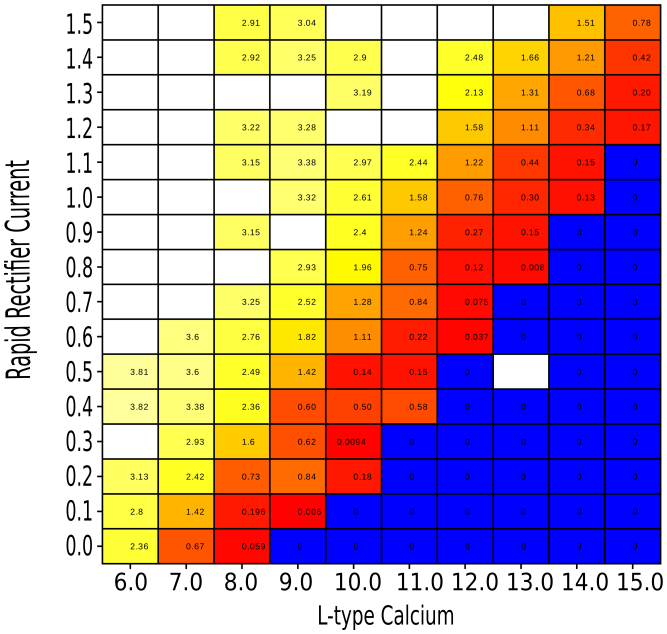


Figure 3.19: Statistical results η for a thresholdvalue at -60 mV and 2048 ms of simulation time for S1 pacing data

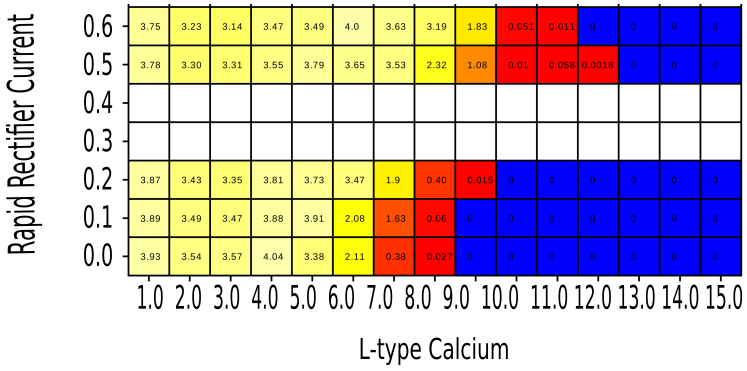


Figure 3.20: Statistical results η for a thresholdvalue at -60 mV and 2048 ms of simulation time for S1S2 data

F. Phase waves versus real waves

As in [8], we made a distinction between real waves and phase waves. Real waves were defined as conventional activation waves. They arise due to the interplay of the excitability of the tissue and diffusion. Real waves travel with a velocity proportional to the square root of the diffusion constant. At impermeable boundaries they are absorbed and do not go through regions in which the tissue is in a refractory state [38]. Phase waves are determined by the pseudo-travelling character they posses and often occur in oscillatory media [38]. They do not depend on the diffusion constant and are not hindered by impermeable boundaries. Therefore, we placed impermeable walls in 3 orthogonal direction. Such walls should stop propagation of normal waves but should not affect phase wave propagation. The results of this simulations are shown in Figure 3.21. We see that for SFb and SFa the waves are hindered by the walls and eventually disappear. We can therefore say they are mediated by normal waves. For the Osc regime, the walls did not significantly affect wave propagation. They are mediated by phase waves. We started these simulations on the final state of the S1 pacing data (after 6048 ms simulation time). Based on the different behaviour after imposing the walls, we classified the SFa and Osc type patterns (Figure 3.5).

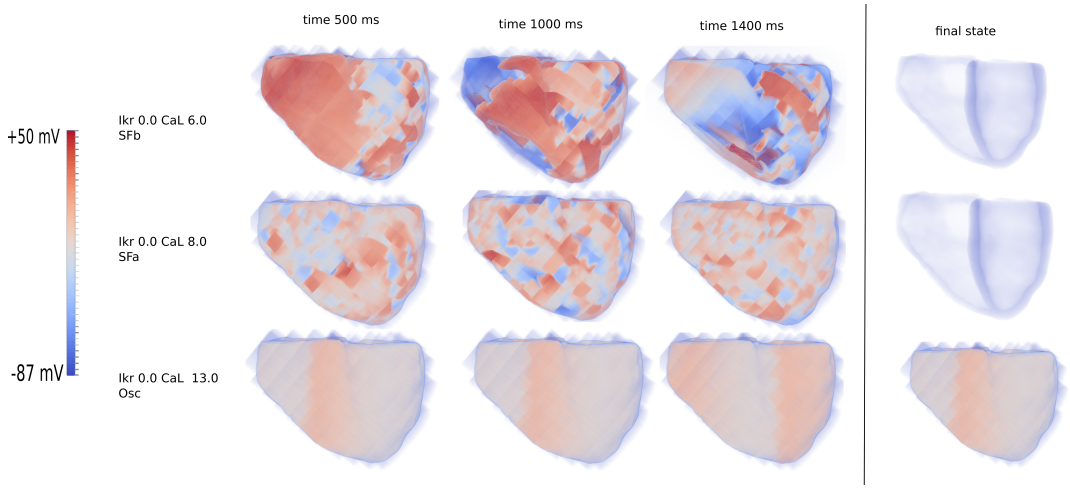


Figure 3.21: Decoupling of the heart along orthogonal planes We represented the decoupling of the three patterns for I_{KR} set to 0.0 and I_{Ca_L} = 6.0, 8.0 and 13.0 times the default.

G. Fourier transforms

For this data-analysis, we considered the same 3016 heartpoints of section E. Of these heartpoints, we took the AP and subsequently the temporal fourier transforms. The average fourier transform is represented in Figure 3.22 in terms of frequency and period. The data of the S1 pacing protocol was used to get this figure. The data of the S1S2 protocol results in the same gradually change of the fourier transforms when I_{Ca_L} is increased. We observe in the

Osc graph a prominent peak at 5 Hz, in accordance with the period of the oscillating AP in graph g of Figure 3.10. The period is 200 ms, corresponding with a frequency of 5 Hz and the average distance between subsequent peaks in the AP. We see this peak as the most prominent peak of the inverse fourier transform. In the graph of SFb we mostly see a prominent peak at 1.94 Hz and 3.88 Hz, corresponding with the periods of 515 ms and 258 ms of the SFb AP in graphs a, b and c of Figure 3.10. The graphs for SFb and Osc resemble strongly the results from Figure 2.5 in section 4 of chapter 2. When the third peak of the fourier transforms became equally or more pronounced then the first two, we classified it as SFa. Based on this global fourier transform of the 3016 heartpoints, we subdevided our results concerning the SFa and SFb patterns (Figure 3.5).

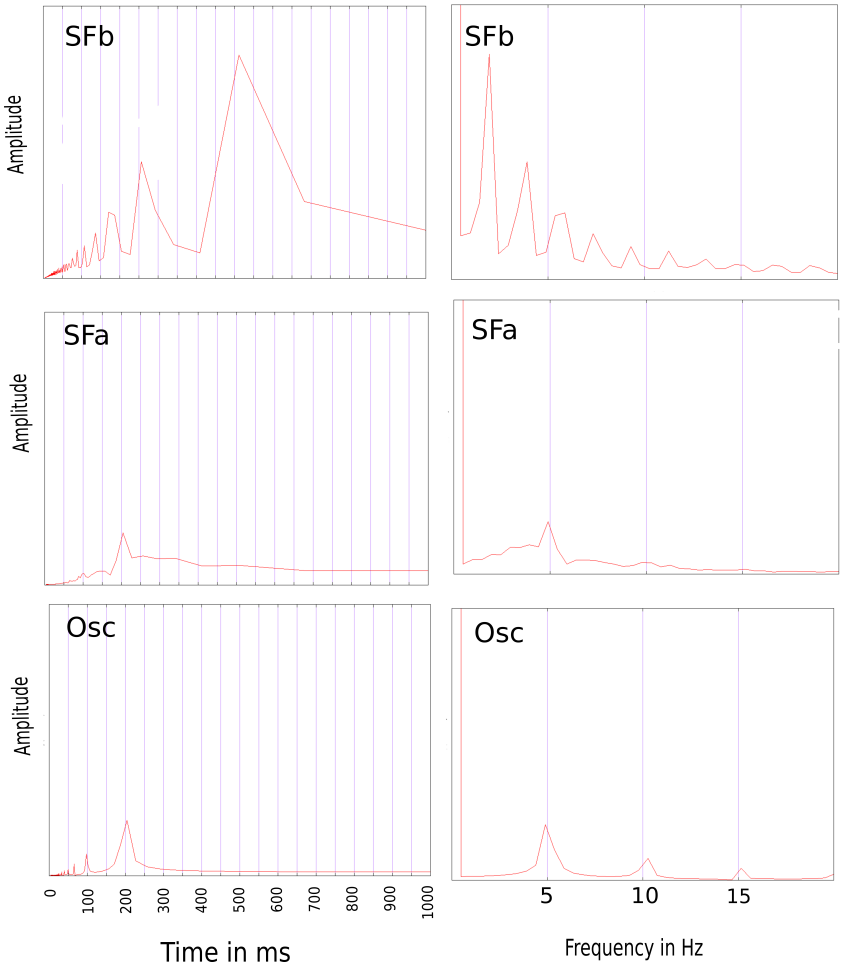


Figure 3.22: Fourier transform and inverse of the transform We show the temporal fourier transform in terms of frequency and period for $I_{KR} = 0.6$ and $I_{Ca_L} = 8.0$, 11.0 and 13.0 corresponding with SFb, SFa and Osc.

H. ECGs

With the software obtained in collaboration with the research group of Professor Seemann, we were able to create the ECGs of the excitation patterns. We performed long simulations of 10 seconds of the three patterns. With a gradual increase of I_{Ca_L} we saw the amplitude of the signals decrease, in accordance with the decreasing scale of the amplitude of the APs. We show the ECGs of the SFb, SFa and Osc type corresponding with the parameter values of $I_{KR} = 0.6$ and $I_{Ca_L} = 8.0$, 11.0 and 13.0 times the default values respectively in Figures 3.23, 3.24 and 3.25. We also illustrated for scale the I-lead of SFb, SFa and Osc together in Figure 3.26. In this Figure, the decreasing amplitude of the ECG can be clearly seen. The ECGs for SFb and SFa are irregular and resemble that of VF. For the Osc patterns, the ECGs are more regular.

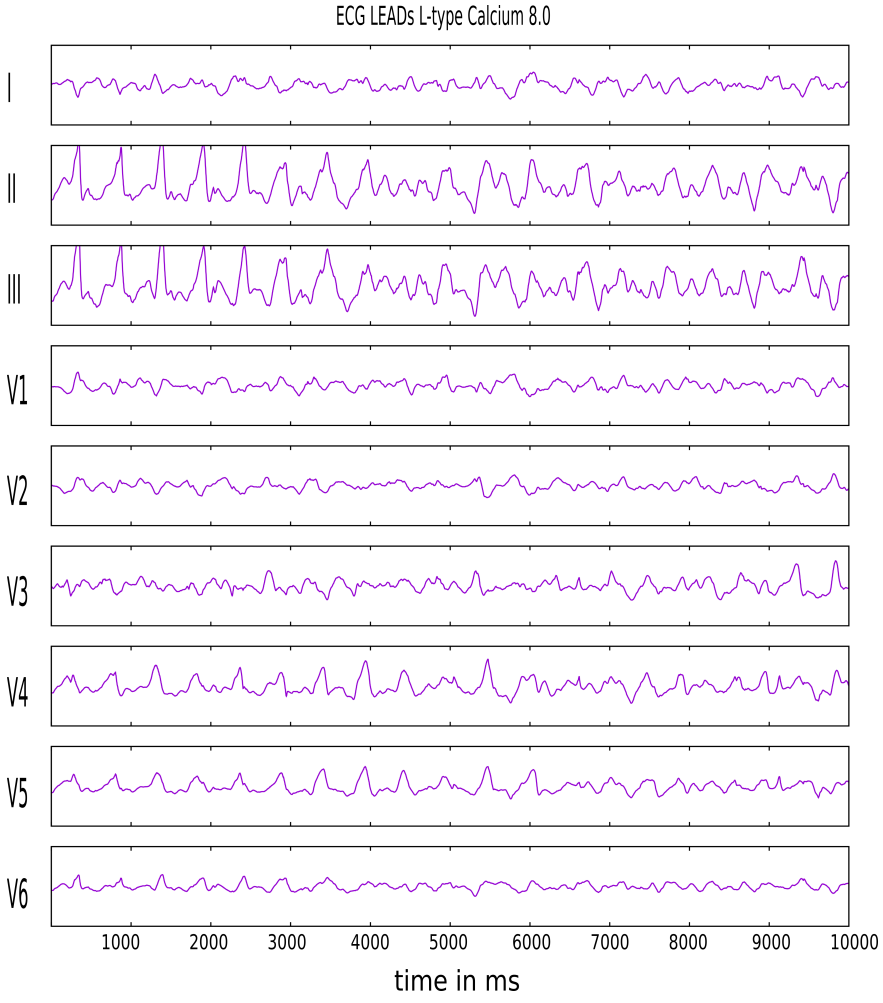


Figure 3.23: ECGs for $I_{KR} = 0.6$ and $I_{Ca_L} = 8.0$, the SFb type

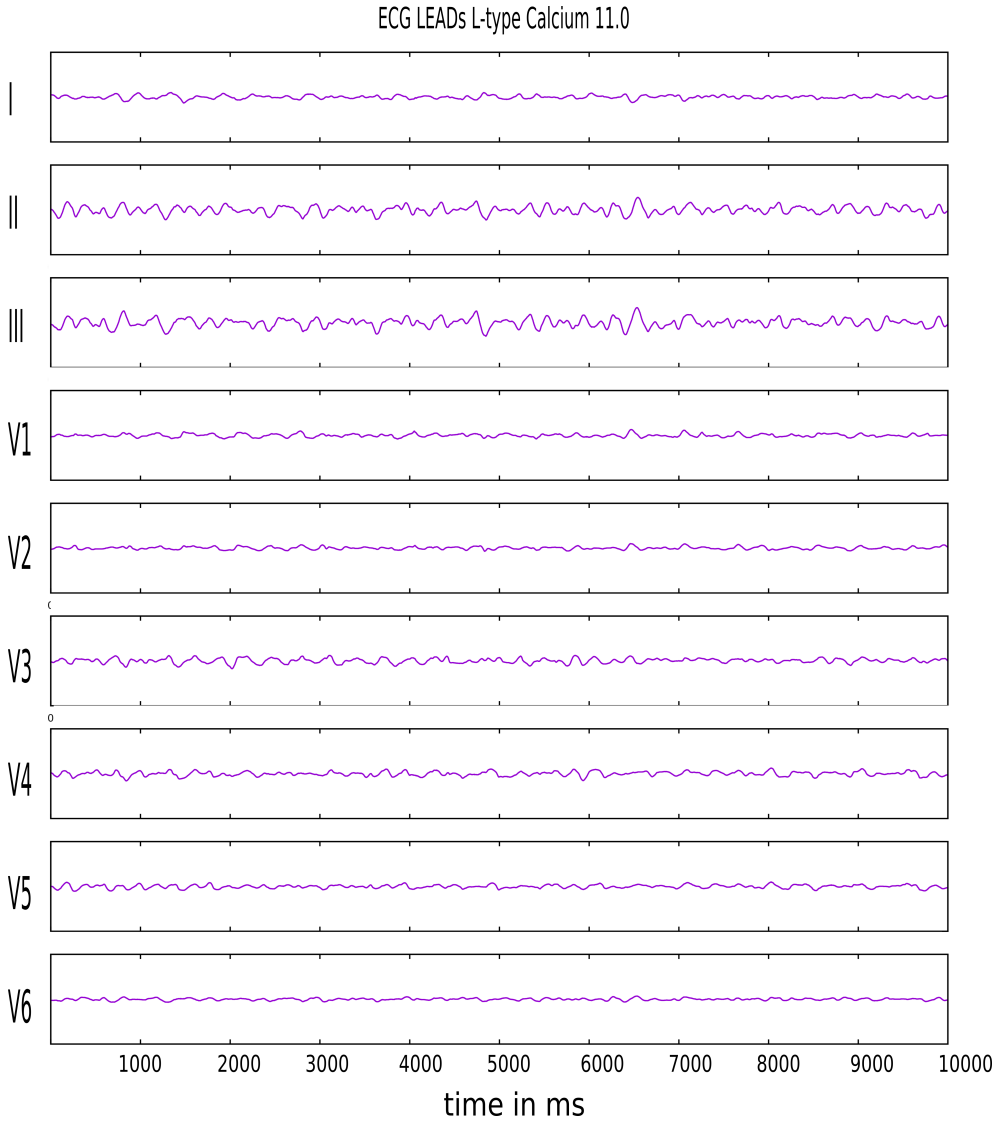


Figure 3.24: ECGs for $I_{KR} = 0.6$ and $I_{Ca_L} = 11.0$, the SFa type

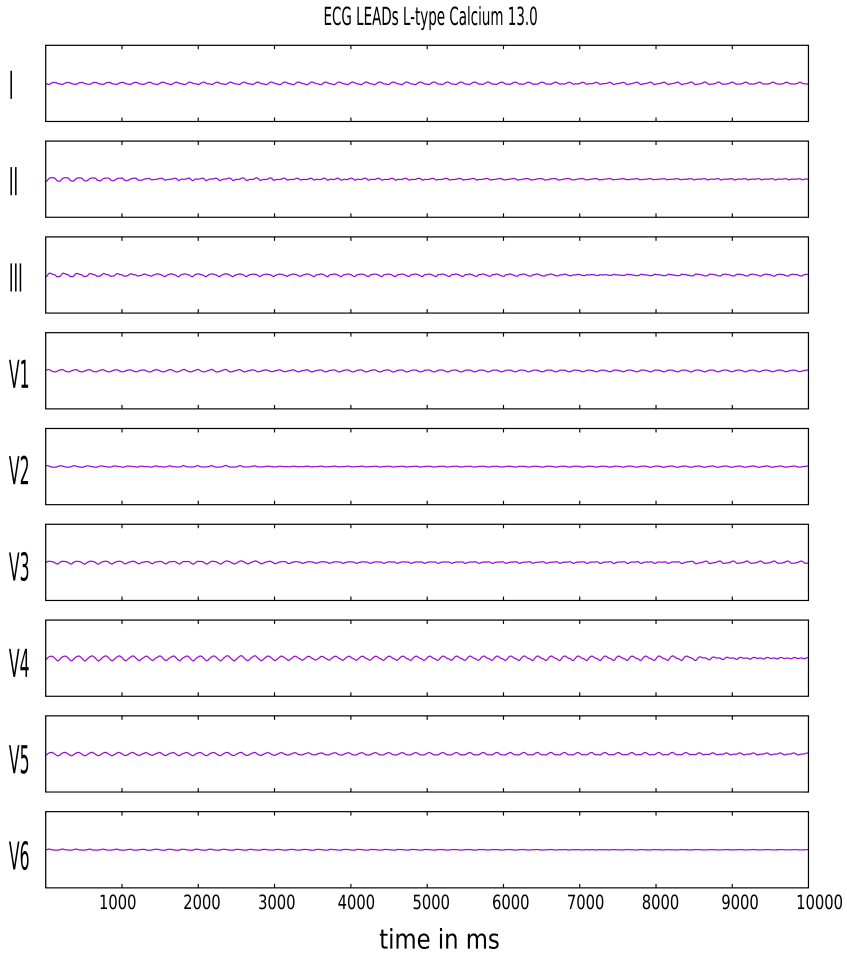


Figure 3.25: ECGs for $I_{KR} = 0.6$ and $I_{Ca_L} = 13.0$, the Osc type

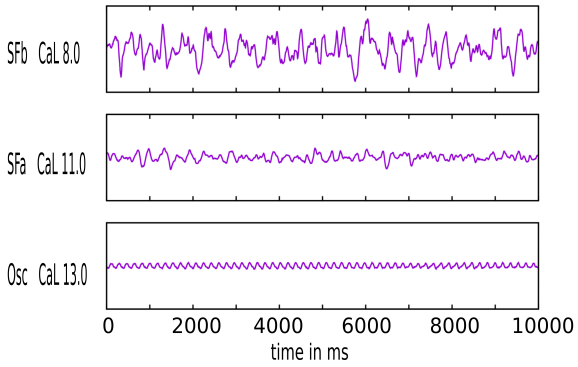


Figure 3.26: ECG I for $I_{KR} = 0.6$ and $I_{Ca_L} = 8.0$, 11.0 and 13.0, respectively SFb, SFa and Osc

4. The meandering spiral

In this section we represented the stable single spiral SSS and the meandering spiral MS. Starting from the SSS at a certain I_{KR} we raised I_{Ca_L}. In the parameter region before the SFb the spiral started to meander. We denoted the region of SSS and MS in pink resp. orange in Figure 3.5.

A. Mechanisms of pattern formation

SSS with S1S2

The inital SSS is created with the S1S2 protocol at $I_{KR} = 1.0$ and $I_{Ca_L} = 1.0$. For this section, we have gradually lowered the I_{KR} value to 0.0 and show the resulting SSS in Figure 3.27, at the beginning of the simulation and at the end after 1500 ms. The center of the spiral remains fixed and the corresponding excitation pattern is therefore called a SSS. We placed in the heart 2 spheres, representing the point from which we took the AP. The AP of the point in the core resp. at the edge is shown in the left resp. right graph of Figure 3.27. We noticed a clear difference between both APs. Even tough the amplitude for the point at the core is small, this is not due to EADs. The APD of this AP is the shortest possible to be sustained in the tissue (Formula 1.15). It has a period around 300 ms. This small amplitude of the AP is only a feature at the core, as the AP further away of the core is normal.

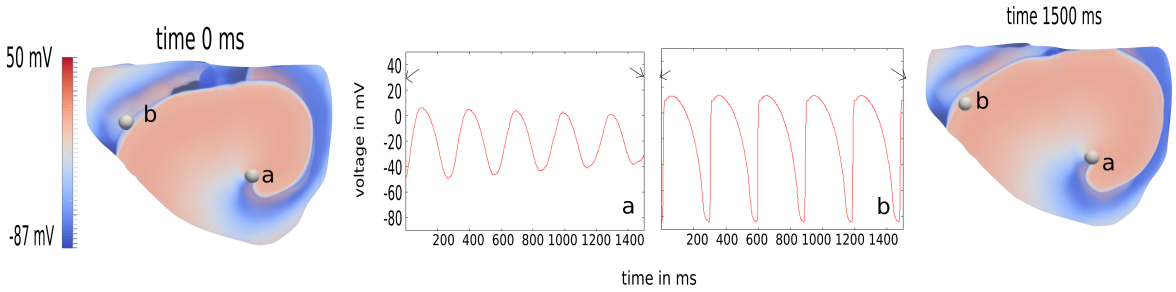


Figure 3.27: Stable spiral from the S1S2-protocol: Timeshots of SSS with parameters $I_{KR} = 0.0$ and $I_{Ca_L} = 1.0$ at the beginning of the simulation (left) and at the end of the simulation after 1500 ms (right). The AP from the marked spheres are shown in the middle. At the left, the AP of the point at the core of the spiral. At the right, the AP of the point on the edge of the spiral.

MS with S1S2

We started from the SSS from previous section. We gradually raised the I_{Ca_L} until 4.0 times the default value and I_{KR} kept at 0.0. We simulated for 1500 ms. At this parameter values, the core of the spiral started to move and we obtained a MS. The cause of the meandering can be associated with EADs. We show this in Figure 3.28. The top row represents timeshots

of the excitation pattern at the beginning, after 700 ms, after 1100 ms and after 1500 ms. The meandering is clearly visible. We recorded the AP of 4 heartpoints denoted with a, b, c and d. Each heartpoint corresponds with the core of the MS at a given timeshot. We see that in the AP of each heartcell EADs emerge at the time the core passes the point. The AP at larger distance from the core, shows a regular AP as can be seen in Figure 3.29.

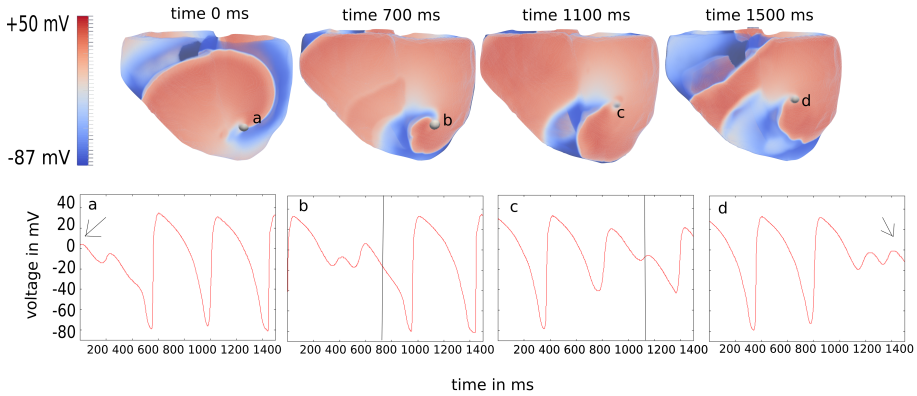


Figure 3.28: S1S2 protocol: EADs inducing MS Top: 4 timeframes of the MS with parameters set to I_{KR} =0.0 and I_{Ca_L} = 4.0 after 0, 700, 1100 and 1500 ms. Buttom: AP of point a,b,c and d shown in respectively graph a,b,c,d.

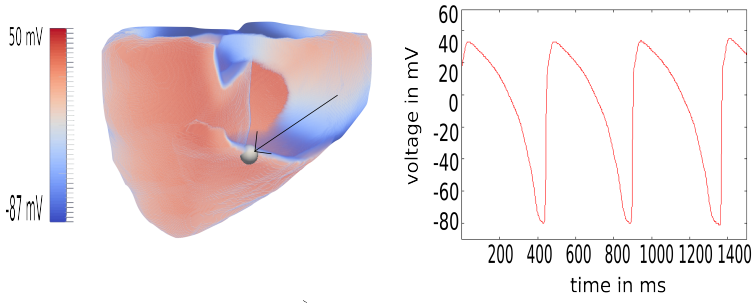


Figure 3.29: S1S2 protocol: opposite side of the core: Timeshot at t = 1500 ms and AP at the point, denoted with the sphere. The parameter values are for I_{KR} = 0.0 and for I_{Ca_L} = 4.0.

B. ECGs of the meandering spiral

From the MSs of Figure 3.5, we performed long simulations of 10 upto 20 seconds. From this, we calculated ECGs. We illustrated the ECG of the MS for I_{KR} = 0.0 and I_{Ca_L} = 4.0 in Figure 3.30. Also the ECG of I_{KR} = 0.1,0.2,0.5 and 0.6 are shown in Figure 3.31. The corresponding I_{Ca_L} values are denoted in the Figure. The ECGs resemble the signature of the arrhythmia TdP.

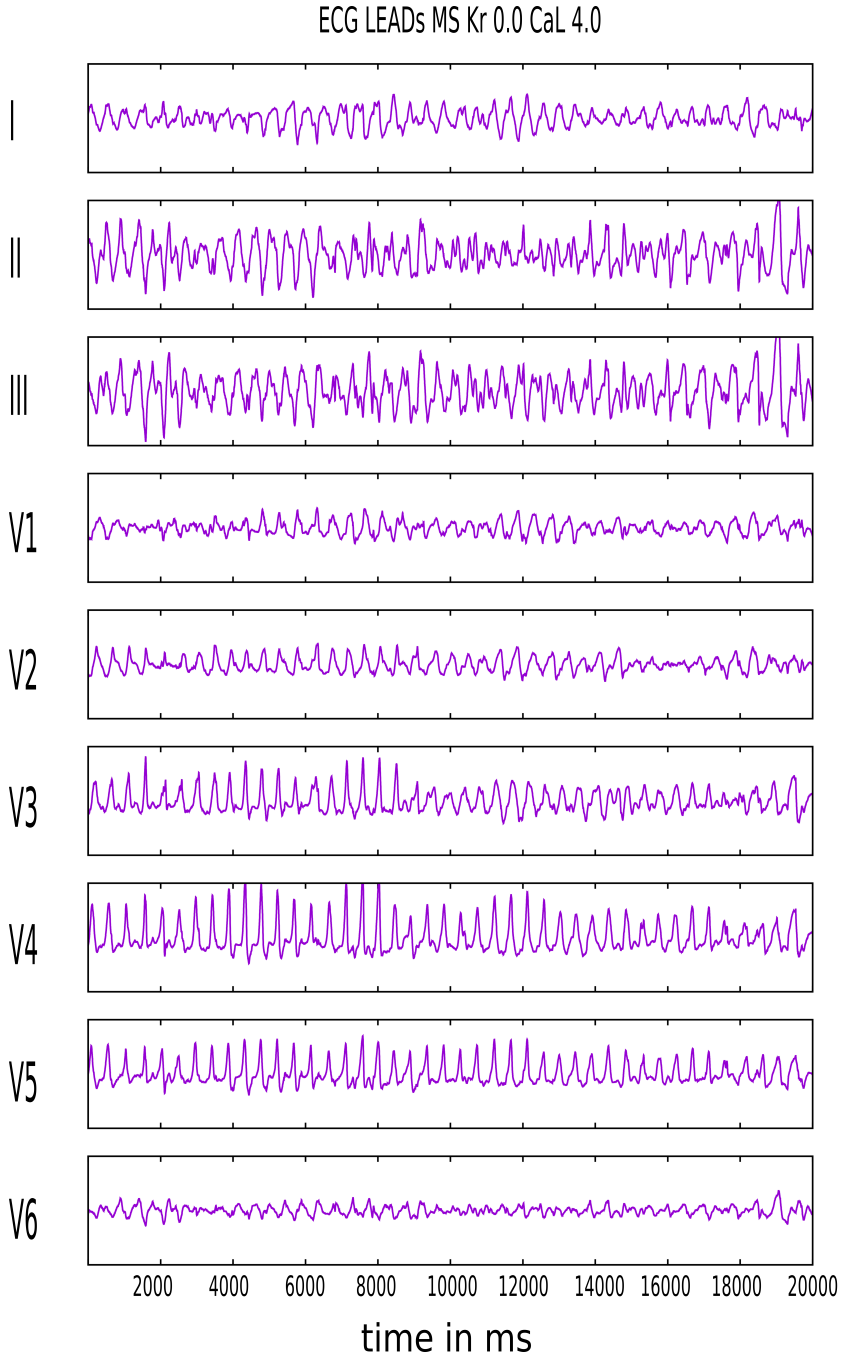


Figure 3.30: ECGs for $I_{KR} = 0.0$ and $I_{Ca_L} = 4.0$ We illustrate the ECGs of the MS for $I_{KR} = 0.0$.

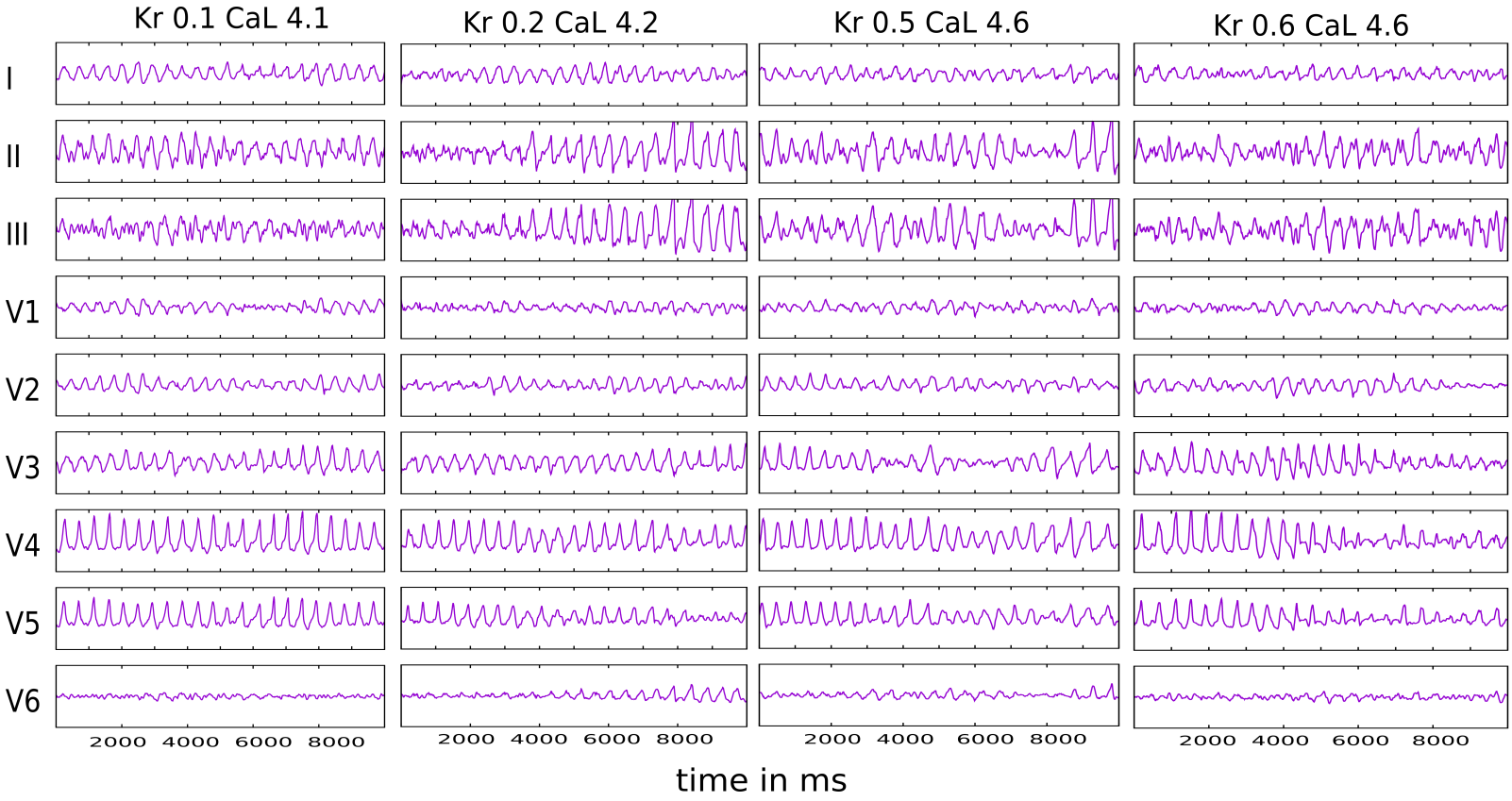


Figure 3.31: ECGs for different probed parameters We illustrate the ECGs of the MS for $I_{KR} = 0.1$, 0.2, 0.5 and 0.6 and I_{Ca_L} 4.1, 4.2, 4.6 and 4.6 resp.

Chapter 4

Discussion

In the industrialized world, cardiac arrhythmias and sudden cardiac death are among the most common causes of death. Theoretical studies into the mechanisms of cardiac arrhythmias form a well-established area of research as the simulation of the human heart can overcome some of the problems manifested in experimental and clinical research (limitations on studies involving human hearts, limited surface recordings,..). Disturbances in the normal propagation of the excitation wave, causes abnormal excitation patterns which can lead to arrhythmias. One such cause, is the emergence of EADs. An EAD is a depolarization phase before complete repolarization [28–30]. They can emerge in the heart, due to genetic defects such as the long QT syndrome [20–22] or due to heart failure [26, 27]. Also pharmacological agents can result in cardiotoxicity [19, 23, 25] and several other conditions [19, 25] can lead to EADs. EADs can influence the heartrhythm by producing ectopic beats. As ectopic beats are known to increase the arrhythmogenicity, EADs are prone to induce heartarrhythmias. Also, as EADs disrupt a homogenous spreading of the electrical wave, they raise the electrical heterogeneity which is also a well known arrhythmogenic condition [17, 18]. During several decades, the computational research on EADs has mainly investigated the behaviour of the EADs on the single cell level. As arrhythmias emerge on the tissue and whole heart level, it is however very important to study the effects of EADs on 1D, 2D and 3D tissues.

This study has focussed on the the spatial patterns due to EADs in the whole heart on an anatomically correct model of the human ventricles: the TNNP-TP06 model. A first part of this thesis was the systematical study of the spatial patterns by reducing I_{KR} and increasing I_{Ca_L}. These variables defined a 2D parameter space. A thorough study in 2D [8] investigated the ranges in which different patterns emerged. This resulted in the classification of three patterns SFb, SFa and Osc. In 3D, we found likewise results and each pattern is characterized with its own features.

The SFb-, SFa- and Osc-type excitation patterns in 3D.

With the aid of the S1S2 pacing protocol we were able to create a stable spiral. Increase of I_{Ca_L} created local and temporal heterogeneities of EADs in the heart. Where a temporal island emerged, the wave broke up or lost speed. This resulted in the creation of eventually 2 spirals around the obstacle or a backwards reflected wave. Further increase resulted in an increasing likelihood of these island and multiple wave-breaks resulted in the SFb pattern. With the S1 pacing protocol islands of EADs emerged at the intensively paced regions at the edge of the S1-pulse. Due to the wave-breaks, pattern formation emerged and we were able to create the three patterns. Different as in [8], also SFb-type patterns were created with the aid of the S1 pacing protocol.

SFb

The SFb-type patterns show a complex spatio-temporal pattern on the large scale of the heart. Bistable waves try to push the heartcells from the equilibrium in the repolarized state to an excited depolarized state. The waves are Calcium- and Sodium mediated and emerge due to an interplay between the excitability of the cells and diffusion. As this defines real waves, impermeable walls absorbed the waves. The typical temporal fouriertransform of multiple heartcells shows waves of large periods around 515 ms. They can be found in the characteristic AP. The ECG of the SFb-type patterns can be associated with VF.

SFa

The SFa-type consists out of interacting rotating spirals and waves. In contrast to the patterns of SFb, the SFa-waves are mostly mediated by Calcium waves but are also absorbed by the impermeable walls. The likelihood of complete repolarization after multiple small EADs in the AP of the cells becomes very small, in accordance with the small amplitude of the waves in the excitation patterns. The amplitude of the ECG is reduced and clearly resembles the ECG of VF.

Osc

The excitation pattern of the Osc-type patterns is imposed by the applied pulses. In contrast to the waves in the SFb- and SFa-type, the waves mediating the excitation pattern of the Osc-type patterns are phasewaves. Impermeable walls do not hinder the waves. The heartcells are oscillators and the spatio-temporal patterns arise due to a shift in the phase of these oscillators. The AP of the oscillators is bounded by a small amplitude around an equilibrium voltage. The period of the oscillating AP emerges from the temporal fouriertransforms at 5 Hz (1/200 ms). Within the research of arrhythmias, knowledge of this Osc- regime is of great relevance as in [17], it has been shown that cardiac myocytes can exhibit electrical

oscillations. They showed that focal activity of these myocytes organized the spatial patterns on an anatomical model of the rabbit heart.

The meandering spiral and Torsade de Pointes

During the second part of this thesis, we focussed on the behaviour of the meandering spiral and its signature on the 12-leads ECG. By increasing I_{Ca_L} starting from a stable spiral, we found close to the parameter region of the SFb type, that the spiral meandered. This meandering was recorded by the 12-leads ECG and resulted in a TdP-like signal for multiple values of I_{KR}. After the meandering, the spiral broke up due to EADs which created multiple spirals and backwards reflected waves. We searched for the origin of the meandering and found EADS at the moving core. We illustrate this again in Figure 4.1. We followed the moving core and the spheres denote the heartpoints of which we took APs. The moment the core passes the spheres, EADs are clearly visible in the AP.

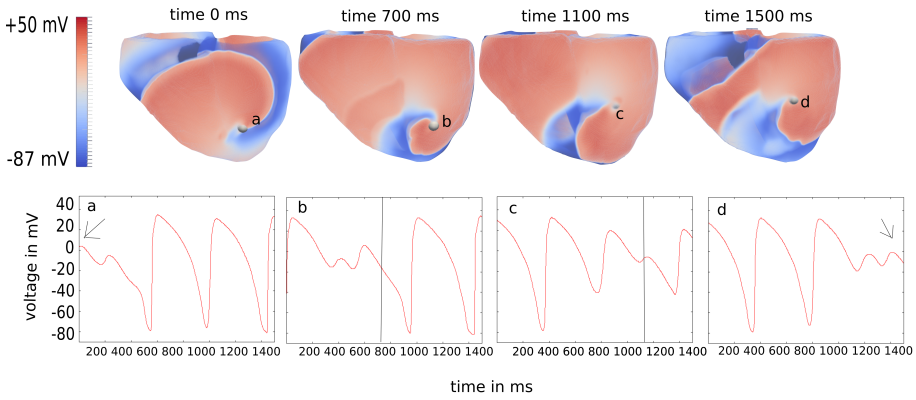


Figure 4.1: EADs accompany the meandering core (for $I_{KR} = 0.0$, $I_{Ca_L} = 4.1$)

Most interesting results are the ECGs of these meandering spirals. We showed in the Results section an overview of the probed regions in which we found the meandering spiral and for which we found ECGs resembling the signal of TdP. This is the first study where in homogeneous tissue signals of TdP are found. TdP-like signals were found due to excitation patterns in a heterogeneous human heart [32] before. In that study, they added islands of M-cells which initiated moving reentrant waves. In Figure 4.2 we illustrated the meandering of the spiral and the corresponding ECG. We also showed the ECG of TdP in this Figure. We noticed the similarities.

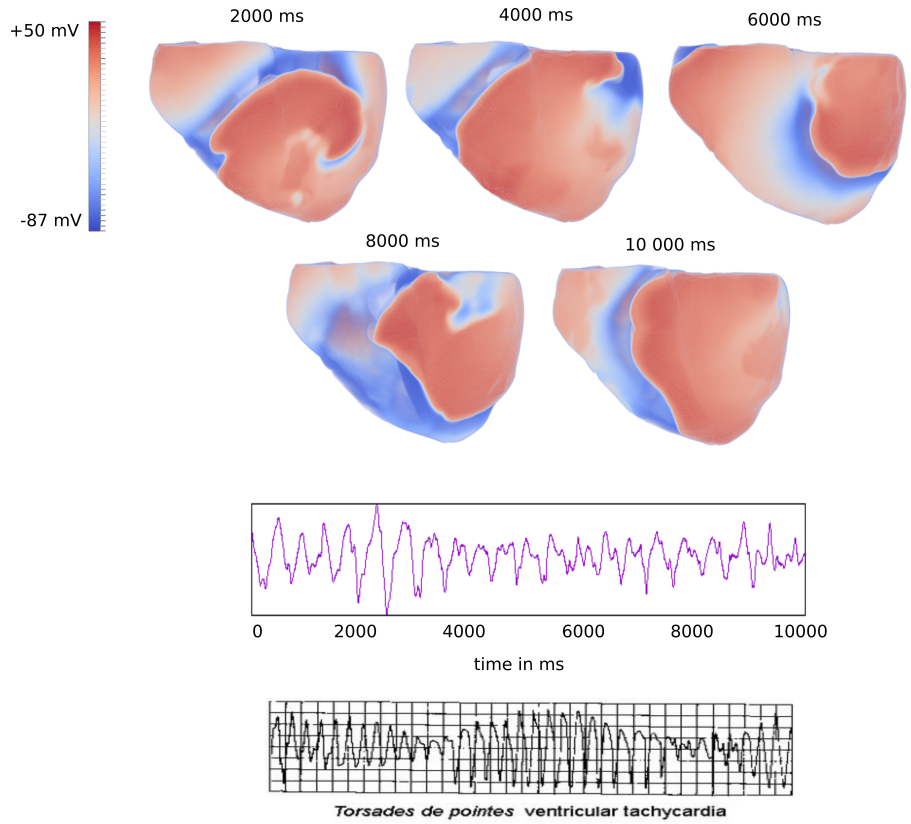


Figure 4.2: The meandering spiral accompanied with its ECG and the ECG of TdP (for $I_{KR} = 0.1$, $I_{Ca_L} = 4.2$)

Bibliography

[1] A. V. Panfilov. *Waves and patterns in biophysics.*

[2] Edward P. Walsh, Mark E. Alexander, and Frank. Cecchin. Electrocardiography and Introduction to Electrophysiologic Techniques. *Nadas' Pediatric Cardiology*, pages 145–181, 2006.

[3] W R Ashby. The Physiological Basis of the Neuroses. *Proceedings of the Royal Society of Medicine*, 26(11):1454–1460, 1933.

[4] Guyton and Hall. *Textbook of Medical Physiology.* Eleventh edition.

[5] A. L. Hodgkin and A. F. Huxley. A quantitative description of membrane current and its application to conduction and excitation in nerve. *The Journal of Physiology*, 1952.

[6] K H W J ten Tusscher, D Noble, P J Noble, and A V Panfilov. A model for human ventricular tissue. 2004.

[7] K H W J ten Tussher and A V Panfilov. Alternans and spiral breakup in a human ventricular tissue model. 2006.

[8] Vandersickel N., Kazbanov I.V., Nuitermans A., Weise L.D., Pandit R. and Panfilov A.V. A Study of Early Afterdepolarizations in a Model for Human Ventricular Tissue. 2014.

[9] A. L. Hodgkin, A. F. Huxley, and B. Katz. Measurement of current-voltage relations in the membrane of the giant axon of Loligo. *Journal of Physiology*, pages 424–448, 1952.

[10] A. F. Huxley and A. L. Hodgkin. The dual effect of membrane potential on sodium conductance in the giant axon of Loligo. *Journal of Physiology*, pages 497–506, 1952.

[11] A F Huxley and A. L. Hodgkin. The components of membrane conductance in the giant axon of Loligo. *Journal of Physiology*, pages 473–496, 1952.

[12] A F Huxley and A. L. Hodgkin. Currents carried by sodium and potassium ion trough the membrane of the giant axon of Loligo. *Journal of Physiology*, pages 449–472, 1952.

[13] Declan A Doyle, Morais Cabral, Richard A Pfuetzner, Anling Kuo, Jacqueline M Gulbis, Steven L Cohen, Brian T Chait, and Roderick Mackinnon. The Structure of the Potassium Channel : Molecular Basis of Conduction and Selectivity. *Science*, 280(April), 1998.

[14] Roden DM, Yang T. *Circulation* 112,1376-1378,2005 Protecting the heart against arrhythmias: potassium current physiology and repolarization reserve

[15] Roden DM *Pacing Clin Electrophysiol* 21:1029-1034 Taking the "idio" out of "indiosyncratic": predicting Torsade de Pointes

[16] Roden DM *Circulation* 118,981-982,2008 Repolarization reserve: a moving target.

[17] Sato D., Xie LH, Sovari AA, Tran DX, Moriat N, et al. *Proc Natl Acad Sci U S A* 106:2983-2988, 2009 Synchronization of chaotic early afterdepolarizations in the genesis of cardiac arrhythmias

[18] Antzelevitch C, Sicouri S. *J Am Coll Cardiol* 1994, 23: 259-277 Clinical relevance of cardiac arrhythmias generated by afterdepolarizations: role of M cells in the generation of U waves, triggered activity and Torsade de Pointes

[19] P.G. Volders, M.A. Vos, B. Szabo, K.R. Sipido, S.H. de Groot, A.P. Gorgels, H.J. Wellens, R. Lazzara *Cardiovasc Res* 46 (3) (2000) 376-392 Progress in the understanding of cardiac early afterdepolarizations and torsades de pointes: time to revise current concepts

[20] Morita H, WU J, Zipes DP *Lancet* 372:750-763 The qt syndromes: long and short

[21] Keating MT, Sanguinetti MC *Cell* 104:569-580 (2001) Molecular and cellular mechanisms of cardiac arrythmias

[22] Liu GC, Choi BR, Ziv O, Li W, de Lange E, et al. *J Physiol* 590: 1171-1180 (2012) Differential conditions for early after-depolarizations and triggered activity in cardiomyocytes derived from transgenic lqt1 and lqt2 rabbits.

[23] Kannankeril P, Roden DM, Darbar D *Pharmacol Rev* 62: 760-781 (2010) Drug-induced long qt syndrome

[24] Liang P, Lan F, Lee A.S., Gong T., Sanchez-Freire V., et al *Circulation* 127 1677-1691 (2013) Drug screening using a library of human induced pluripotent stem cell-derived cardiomyocytes reveals disease-specific patterns of cardiotoxicity.

[25] Sipido KR., Bito V., Antoons G., Volder P.G., Vos M.A. *Ann N Y Acad Sci* (2007) 1099: 339-348 Na/Ca exchange and cardiac ventricular arrhythmias

[26] Nuss H.B., Kaab S, Kass DA, Tomaselli GF, Marban E. *Am. J. Physiol Heart Circ Physiol* (1999) 277:H80-91 Cellular basis of ventricular arrhythmias and abnormal automaticity in heart failure

[27] Li G.R., Lau C.P., Ducharme A., Tardif J.C., Nattel S. *Am. J. Physiol. Heart Circ. Physiol* 283: H10 31-41 Transmural action potential and ionic current remodeling in ventricles of failing canine hearts.

[28] Cranefield PF *Circ Res* 41: 415-423 (1977) Action potentials, afterpotentials and arrhythmias

[29] Roden D.M., Viswanathan P.C. *J Clin Invest* 115: 2025-2032 (2005) Genetics of acquiered long qt syndrome

[30] Qu Zl., Xie L.H., Olcese R, Karagueuzian H.S., Chen P.S., Garfinkel A., Weiss J.N. *Cardiovasc Res* (2013) Jul 1; 99(1): 6 -15 Early afterdepolarizations in cardiac myocytes: beyond reduced repolarization reserve

[31] Axel Loewe,Walther H. W. Schulze,Yuan Jiang,Mathias Wilhelms,Armin Luik,Olaf Dossel and Gunnar Seemann Hindawi Publishing CorporationBioMed Research InternationalArticle ID 530352 ECG-Based Detection of Early Myocardial Ischemia ina Computational Model: Impact of Additional Electrodes,Optimal Placement, and a New Feature for ST Deviation

[32] D.F. Richards, J.N. Glosli, E.W. Draeger, A.A. Mirin, B. Chan, J.-L. Fatteberg, W.D. Krauss, T. Oppelstrup, C.J. Butler, J.A. Gunnels, V. Gurev, C. Kim, J. Magerlein, M. Reumann, H.-F. Wen, J.J. Rice *Comput Methods Biomech Biomed Engin* 16 (7) (2013) 802-805 Towards real-time simulation of cardiac electrophysiology in a human heart at high resolution

[33] N. Vandersickel, E. Van Nieuwenhuyse, A.V. Panfilov Spatial Patterns due to Early Afterdepolarizations

[34] Bernus P, Wilders R, Zemlin CW, Verschelde H and Panfilov AV *Am J Physiol Heart Circ Physiol* 282 H2296-H2308 (2002) A computationally efficient electrophysiological model of human ventricular cells

[35] Tusscher KHWJT, Panfilov AV *Am J Physiol Heart Circ Physiol* 284 H542-H548 Reentry in heterogeneous cardiac tissue described by te luo-rudy ventricular action potential model

[36] Rush S and Larsen H. *IEEE Trans Biomed Eng* 25 389-392 (1978) A practical algorithm for solving dynamic membrane equations

[37] Chang MG, Sato D, de Lange E, Lee JH , Karagueuzian HS, et al *Heart Rhythm* 9 115-122 (2012) Bistable wave propagation and early afterdepolarization-mediated cardiac arrhythmias

[38] Tyson JJ, Keener JP *Physica D* 32: 327-361 Singular perturbation theory of traveling waves in excitable media (a review)

List of Figures

1.1 Comparison of the AP of the pacemaker cells and normal cardiac cells. The pacemakercells depolarize spontaneously. The normal cardiac cells need an external applied stimulus or electrical pulse in order to push them over excitation threshold. 2
1.2 Anatomical pathway of spreading of the electrical excitation wave from AV-node to ventrical cardiac tissue, from Medical Physiology, Guyton and Hall. 2
1.3 Spreading of the electrical excitation wave from AV-node to ventrical cardiac tissue, from Waves and patterns in biophysics, A. Panfilov. 3
1.4 Illustration of the influence of potassium and sodium on the global formation of the AP. 5
1.5 Equivalent electrical circuit representing the dynamics of the membrane. Resistances R_{Na} and R_K are time and membrane potential dependent, R_L is constant, from the original paper of A. L. Hodgkin and A. F. Huxley 7
1.6 A, raising g_K associated with depolarization. B, reducing g_K associated with repolarization of the membrane, from the original paper of A. L. Hodgkin and A. F. Huxley. 9
1.7 Left: Determination of the dependency of the potassium channels on both voltage and time; the time scale applies to all records, the ordinate scale is the same in the upper ten curves (A to J) and is increased fourfold in the lower two (K and L), the number is the depolarization in mV. Right: Determination of the dependency of the sodium channels on both voltage and time, the time scale applies to all records, the ordinate scale is the number of the depolarization in mV. From the original paper of A. L. Hodgkin and A. F. Huxley. 9
1.8 Illustration of step 1, 2 and 3 in the formation of the AP, from Waves and patterns in biophysics, A. Panfilov 11
1.9 Simplified representation of the influence of the sodium and potassium channels, from Waves and patterns in biophysics, A. Panfilov 12
1.10 Main currents responsible for the typical form of the cardiac AP. The direction of the arrows denotes if the current is either outwards or inwards. 13

1.11 Representation of the different aspects responsible for the complex dynamics of calcium in the cardiac cell. 14
1.12 Illustration of an EAD. 16
1.13 Left: Illustration of the refractory period after the passage of an exciting wavefront. Right: the annihilation of wavepropagation due to colliding fronts, from Waves and patterns in biophysics, A. Panfilov. 18
1.14 The action potential of the pacemaker cells and normal cardiac cells. 19
1.15 An illustration of competing spherical sources. 19
1.16 Spiralwave creation around and without an obstacle, resp. left and right, from Waves and patterns in biophysics, A. Panfilov. 19
1.17 Illustration of the PQRST-signature, from Medical Physiology, Guyton and Hall. 20
1.18 The AP of a single cardiac cell, left, and the creation of the PQRST-signature on cardiac level due to this AP, right, from Medical Physiology, Guyton and Hall 21
1.19 From top to bottom, illustration of the ECG of a ventricular ectopic beat VPC, Ventricular Tachycardia VT, Atrial Fibrillation AF and Ventricular Fibrillation VF, from Advanced methods and tools for ECG data analysis, Andrew T. Reisner, Gari D. Clifford, and Roger G. Mark. 23
1.20 Schematical representation of the excitation patterns causing arrhythmias, from Waves and patterns in biophysics, A. panfilov. 23
1.21 Illustration of TdP on the ECG. 23

2.1 The used protocols P1 and P2 for the study of EAD in 2D from [8]. 25
2.2 Parametric space of EADs induced spatial patterns SFb, SFa and OscIllustration of the 2D parameter space in which the different types of patterns emerged. [8] 26
2.3 The SFa, SFb and Osc -typeIllustration of the voltage patterns, the output of the Calcium gates and the output of the sodium gates from [8] 27
2.4 Phase waves vs real wavesIllustration of the grid-shaped decoupling of the tissue-sheet where the Osc type move undisturbed through the unpermeable walls, whilst the SFa and SFb type clearly are hinderded by the decoupling, from [8] 28
2.5 Time course characteristicsIllustration of AP, the ECG and the temporal fourier transform of the 3 types, from [8] 28

3.1 Illustration of the S1-pulse. 30

3.2 Parameter range for the S1 pacing and S1S2 protocol.We illustrated the probed parameter range for both protocols. S1S2:The pink square represents the default values of the TNNP-TP06 model, whereby the stable spiral was created. Starting from here, we lowered and raised I_{KR} until the spiral settled. We then followed the blue arrows by raising I_{Ca_L} gradually until the pattern stabilized in the new parameter region. S1 pacing: The parameter ranges for 10 S1 pulses is shown in red. Parameter values for which we paced only once are denoted in yellow. 31
3.3 Creation of the single stable spiral at the default parameters with the S1S2-protocol.At the left: the S2 pulse after the passing of the S1 pulse from Figure 3.1. At the right: the resulting stable spiral at the default values. 32
3.4 Torso with the applied electrodes. Blue electrodes are needed for the collection of ECGs used during this thesis, from [31]. 32
3.5 Classification of the 5 different type of patterns with the S1S2 protocol (left) and with the S1 pacing protocol (right). We denoted the range of the single stable spiral SSS, the meandering spiral MS and the three patterns SFb, SFa and Osc. 34
3.6 SFb patternEvolution of the SFb pattern with the S1 pacing protocol for I_{KR} = 0.6 and I_{Ca_L} = 8.0 times the default values. 35
3.7 SFa patternEvolution of the SFa pattern with the S1 pacing protocol for I_{KR} = 0.6 and I_{Ca_L} = 11.0 times the default values. 35
3.8 Osc patternIllustration of the Osc pattern for both the S1 pacing as the S1S2 protocol. We saw a difference due to the differing initial applied pulse. . . . 36
3.9 Cross-section of the heartCross-section of the excitation pattern in the heart for the three patterns for I_{KR} = 0.6 and I_{Ca_L} = 8.0, 11.0 and 13.0 times the default. 36
3.10 Typical AP for SFb, SFa and OscIn this figure we illustrated the typical AP of the three patterns. We saw a gradual transition from SFb to SFa into Osc by the decrease of the amplitude through the APs. 37
3.11 Increment of the complexity of the spatio-temporal patternWe show the increase of the I_{Ca_L} from 4.0 to 5.0 in steps of 0.2. The meandering spiral breaks up gradually and eventually results into an SFb pattern. 38
3.12 Transition from the SFb to the Osc exciation patternWe illustrate the step-by-step increase of I_{Ca_L} and the corresponding excitation pattern, contineously changing from SFb into SFa to Osc. The number denotes I_{Ca_L}. 38
3.13 Backwards moving waveAn illustration of a backwards moving wave. 39
3.14 EADs at the meandering coreWe illustrate the raised complexity at the core due the EADs breaking the excitation pattern into 2 spirals. 39

3.15 S1 pacing: EADs creating the SFb-patternWe illustrated the heart between the 4th and 5th S1pulse after 2120 ms simulation time. The graph illustrates the AP of the cell marked with the arrow. 40
3.16 SFa pattern induced by EADsWe illustrated timeshots after 1600, 2400 and 4000 ms. We show the AP of the points in a and b. 41
3.17 S1 pacing in the oscillatory regionAfter applying the first S1-pulse, the cells failed to repolarize and followed an oscillatory regime. 41
3.18 Sodium and calcium mediated wavesOn the final states of the S1S2 protocol we simulated another 1000 ms. We illustrated the opening and closing gates of L-type calcium and sodium and the voltage excitation pattern. The scale of the sodium and calcium-output is relative in order to produce the clearest images. 42
3.19 Statistical resultsη for a thresholdvalue at -60 mV and 2048 ms of simulation time for S1 pacing data 43
3.20 Statistical resultsη for a thresholdvalue at -60 mV and 2048 ms of simulation time for S1S2 data 43
3.21 Decoupling of the heart along orthogonal planesWe represented the decoupling of the three patterns for I_{KR} set to 0.0 and I_{Ca_L} = 6.0, 8.0 and 13.0 times the default. 44
3.22 Fourier transform and inverse of the transformWe show the temporal fourier transform in terms of frequency and period for $I_{KR} = 0.6$ and $I_{Ca_L} = 8.0$, 11.0 and 13.0 corresponding with SFb, SFa and Osc. 45
3.23 ECGs for $I_{KR} = 0.6$ and $I_{Ca_L} = 8.0$, the SFb type 46
3.24 ECGs for $I_{KR} = 0.6$ and $I_{Ca_L} = 11.0$, the SFa type 47
3.25 ECGs for $I_{KR} = 0.6$ and $I_{Ca_L} = 13.0$, the Osc type 48
3.26 ECG I for $I_{KR} = 0.6$ and $I_{Ca_L} = 8.0$, 11.0 and 13.0, respectively SFb, SFa and Osc 48
3.27 Stable spiral from the S1S2-protocol: Timeshots of SSS with parameters I_{KR} = 0.0 and I_{Ca_L} = 1.0 at the beginning of the simulation (left) and at the end of the simulation after 1500 ms (right). The AP from the marked spheres are shown in the middle. At the left, the AP of the point at the core of the spiral. At the right, the AP of the point on the edge of the spiral. 49
3.28 S1S2 protocol: EADs inducing MSTop: 4 timeframes of the MS with parameters set to I_{KR} =0.0 and I_{Ca_L} = 4.0 after 0, 700, 1100 and 1500 ms. Buttom: AP of point a,b,c and d shown in respectively graph a,b,c,d. 50
3.29 S1S2 protocol: opposite side of the core: Timeshot at t = 1500 ms and AP at the point, denoted with the sphere. The parameter values are for I_{KR} = 0.0 and for I_{Ca_L} = 4.0. 50
3.30 ECGs for $I_{KR} = 0.0$ and $I_{Ca_L} = 4.0$ We illustrate the ECGs of the MS for I_{KR} = 0.0. 51

3.31 ECGs for different probed parametersWe illustrate the ECGs of the MS for I_{KR} = 0.1, 0.2, 0.5 and 0.6 and I_{Ca_L} 4.1, 4.2, 4.6 and 4.6 resp. 52

4.1 EADs accompany the meandering core (for $I_{KR} = 0.0$, $I_{Ca_L} = 4.1$) 55
4.2 The meandering spiral accompanied with its ECG and the ECG of TdP (for $I_{KR} = 0.1$, $I_{Ca_L} = 4.2$) 56

List of Tables

1.1 Intra- and extracellular concentrations of main ions in mM, from Medical Physiology, Guyton and Hall. 3

3.1 Applied simulationtime for each parameter value probed with the S1S2-protcol. 33